Petrogenic Carbon Oxidation and Its Impact on the Carbon Balance in the Ganga River Basin

Rupak Samadder[1*], Tarun K. Dalai[1], Kruttika Mohapatra[2], Pankaj Kumar[3], Damodararao Karri[4], Sanjeev Kumar[5]

[1]Department of Earth Sciences, Indian Institute of Science Education and Research Kolkata, Mohanpur 741246, India

[2]Department of Earth and Climate Science, Indian Institute of Science Education and Research Pune, Pune 411008, India

[3]Inter-University Accelerator Centre, New Delhi 110067, India

[4]Center for Climate Change Research, Indian Institute of Tropical Meteorology, Pune 411 008, India

[5]Geosciences Division, Physical Research Laboratory, Navrangpura, Ahmedabad 380009, India

*Corresponding author: Rupak Samadder (rupaksamadder@gmail.com)

Peer review status:
This is a non-peer-reviewed preprint submitted to EarthArXiv.

Abstract

Based on sampling and investigation spanning several years, we conduct a comprehensive assessment of petrogenic organic carbon (OC_{petro}) oxidation and evaluate the net carbon budget in the Ganga–Hooghly River (GHR) basin, extending from the Himalayan mountainous catchments to the floodplains in India. Our multi-proxy approach combines data on rhenium (Re) concentrations, radiocarbon (pMC), stable carbon isotopes ($\delta^{13}C_{org}$), major and trace element concentrations to determine Re contributions to the Ganga–Hooghly rivers from different sources. We demonstrate that OC_{petro} is the dominant source across the entire GHR system, accounting for up to 97% of dissolved Re. Such an outcome justifies our approach of determining the CO_2 release from OC_{petro} oxidation by using dissolved Re as a tracer. In the GHR basin, monsoon periods are characterized by the highest CO_2 fluxes from OC_{petro} oxidation, with emissions that match or exceed CO_2 drawdown via silicate weathering. In contrast, this pattern reverses during low-discharge periods. The power-law relationship observed between CO_2 release from OC_{petro} oxidation and sediment yield underscores primary role of physical erosion in controlling OC_{petro} oxidation. We further propose that in mountainous catchments, although carbon release yields are higher, a fraction of OC_{petro} experiences minimal to negligible oxidation. The emission of CO_2 from OC_{petro} oxidation is largely balanced by its consumption via silicate weathering. However, both these fluxes are surpassed by substantial OC_{bio} burial driven by enhanced sediment transport. Consequently, the GHR catchment functions overall as a net sink of atmospheric CO_2.

Keywords

Petrogenic organic carbon; Oxidative weathering; Rhenium; Net carbon balance; Ganga–Hooghly River Basin

1. Introduction

The long-term (10^4-10^6 years) carbon cycle is regulated by coupled geological and biological processes. Over these intervals, the principal sources of atmospheric CO_2 include volcanism, sulfuric acid–mediated weathering of carbonate rocks, and oxidation of petrogenic organic carbon (OC_{petro}). Major CO_2 removal pathways comprise silicate weathering by carbonic acid, carbonate precipitation in the ocean and sedimentary organic carbon (OC) burial (Gaillardet et al., 1999; Galy et al., 2007). Among these processes, oxidative weathering of OC_{petro} represents a direct source of CO_2 and a sink of O_2, as exposure of sedimentary rocks containing OC_{petro} to atmospheric or dissolved O_2 promotes oxidation reactions that consume O_2 and release CO_2 to the atmosphere (Chang and Berner, 1999; Galy et al., 2008a). Rivers play an essential role in these processes by mobilizing and transporting both OC_{petro} and biospheric organic carbon (OC_{bio}). Burial of OC_{bio} constitutes a net sink of atmospheric CO_2, whereas burial of OC_{petro} is effectively carbon neutral on geological timescales. In contrast, oxidation of OC_{petro} releases CO_2, partially offsetting CO_2 consumption driven by silicate weathering.

Oxidation of OC_{petro} is closely coupled to tectonic uplift and physical erosion, processes that exhume reduced sedimentary rocks and expose them to oxygenated surface environments (Hilton et al., 2014; Horan et al., 2017; Zondervan et al., 2023). High physical erosion rates in mountainous regions continuously supply fresh rocks, thereby enhancing OC_{petro} oxidation (Hilton et al., 2014; Horan et al., 2017). However, elevated erosion rates can also reduce residence times within the soil and weathering zones (Hemingway et al., 2018), potentially limiting the degree of oxidation prior to fluvial transport downstream. Thus, physical erosion exerts competing controls on the fate of OC_{petro}, by promoting its exposure and oxidation while enhancing its preservation in

high-erosion settings. In the floodplains, longer residence times, sustained exposure to oxidative conditions and elevated temperatures can collectively enhance the oxidation of OC_{petro} (Bouchez et al., 2010; Dellinger et al., 2023; Galy et al., 2008a). Therefore, comparative studies across these two contrasting settings provide crucial insights into the spatial variability, rates and controls of OC_{petro} oxidation. Such understanding is essential for elucidating how the tectonics-erosion-climate coupling regulating carbon cycling at the Earth's surface. Additionally, such studies are crucial for improving estimates of land–atmosphere carbon fluxes and the predictive capability of carbon cycle models. Despite its importance, the integrated assessment of OC_{petro} oxidation remains poorly constrained in river systems that span both mountainous headwaters and downstream floodplains.

The Ganga- Hooghly River (GHR) system in India is characterized by very high suspended particulate matter (SPM) loads (Abbas and Subramanian, 1984; Rudra, 2014) driven by tectonically induced physical erosion in the upper reaches (Khan et al., 2018; Roy and Sinha, 2017) and intense monsoonal precipitation in the lower reaches (Khan et al., 2018; Lupker et al., 2011; Roy and Sinha, 2017). This combination of factors makes the GHR basin an ideal setting for investigating the processes that regulate OC_{petro} oxidation under both the mountainous and floodplain conditions. The burial of OC in the Bengal Fan has been reported to represent a significant fraction of global OC burial, on the order of 10-20% (Galy et al., 2007). Notably, sediments delivered to the Bay of Bengal exhibit selective preservation of graphitic OC_{petro}, reflecting its resistance to oxidation, whereas non-graphitic OC_{petro} is preferentially oxidized during weathering and transport (Galy et al., 2008a). Globally, physical erosion is recognized as a primary control on the export efficiency of OC_{petro} (Galy et al., 2015). Additionally, studies indicate that as sediments transit through the Ganga River floodplains, their OC composition is

97 modified through addition of biospheric OC, prior to further transport and burial in the Bay of
98 Bengal (Galy et al., 2008b). These observations underscore the dynamic interplay between erosion
99 and oxidation of OC_{petro} in the Ganga River catchment and its subsequent burial in the Bengal Fan.
100 However, despite the Ganga River basin's significance for global sediment and carbon fluxes, a
101 comprehensive, multi-seasonal quantification of OC_{petro} oxidation across both the mountainous
102 upper reaches and the lower floodplains remains lacking.

103 Dissolved rhenium (Re) concentrations in rivers have been used as a proxy of OC_{petro}
104 oxidation to quantify CO_2 release on a basin-wide scale (Dalai et al., 2002; Horan et al., 2019). In
105 suboxic to anoxic conditions, Re is removed from seawater and pore water (Colodner et al., 1993;
106 Crusius et al., 1996) and is incorporated into marine sediments. Uplift and exposure of sedimentary
107 rocks remobilize Re during oxidative weathering, thereby linking dissolved Re fluxes to the OC_{petro}
108 oxidation and associated CO_2 release. Rhenium is considered an effective tracer of OC_{petro}
109 oxidation as (i) it is enriched in OC_{petro} (ii) its dissolved species, ReO_4^-, is stable over a wide pH
110 range (0-14; Brookins, 1986; Nikolaychuk, 2022) and it behaves conservatively in riverine,
111 estuarine and oceanic environments (Colodner et al., 1993; Rahaman and Singh, 2010). Here, we
112 combine multi-seasonal and multi-annual (2012-2020) measurements of dissolved and particulate
113 Re concentrations, stable carbon isotope ($\delta^{13}C_{org}$) and radiocarbon (pMC) compositions of SPM
114 and surface sediments, together with major and trace element compositions, to deconvolve
115 dissolved Re derived from OC_{petro} oxidation from contributions associated with silicate
116 weathering, sulfide oxidation, and anthropogenic inputs. The results of these calculations allow
117 dissolved Re to be used as a tracer to quantify basin-integrated CO_2 fluxes resulting from OC_{petro}
118 oxidation, and to evaluate the net carbon balance of the GHR catchment. Furthermore, we compare
119 OC_{petro} oxidation fluxes with sediment yields across the entire GHR catchment to evaluate the

differences in the modes of OC_{petro} oxidation between the mountainous and the floodplain environments.

2. The Study area

The Hooghly River is a distributary of the Ganga River (Fig. 1a). The Ganga River originates from the Gangotri Glacier in Uttarakhand, India, and flows through the Himalayan range before entering the northern plains at Haridwar. In the plains, the Ganga River is joined by several Himalayan (e.g., the Ghaghra, Gandak, and Kosi) and peninsular tributaries (e.g., the Tons and Son). The Yamuna River, the largest tributary of the Ganga River, drains both the Himalayas and peninsular India (via the Chambal, Betwa, and Ken rivers). At Farakka, the Ganga River bifurcates into the Padma River, which flows into Bangladesh, and the Hooghly River, which flows through West Bengal before discharging into the Bay of Bengal about 200 km downstream of Kolkata. In West Bengal, the Hooghly River is augmented by tributaries, namely the Damodar, the Ajay, and the Rupnarayan rivers.

The Ganga River drains an area of 935×10^3 km^2, distributed among the Himalayas (18%), Peninsular India (37%), and the Gangetic Plains (44%) (Fekete et al., 2004; Singh et al., 2008). The mean annual discharge of the river is 380 km^3/yr at Farakka. The Hooghly River drains an area of 22.5×10^3 km^2 and carries a water discharge of 68.8 km^3/yr at Nabadwip (located ~50 km upstream of Kolkata), with the monsoon period (July-September) accounting for ~50% of the annual water discharge (Rudra, 2014). The annual sediment flux at Kolkata is 328×10^6 tons/yr (Abbas and Subramanian, 1984), representing ~45% of the Ganga River sediment flux at Farakka, where the river accounts for ~20% of the Ganga River water discharge.

The Hooghly River is part of the G-B system, which forms the world's largest delta. The river basin is characterized by thick sedimentary successions (Allison et al., 2003; Mukhopadhyay et al., 2023). These sediments, composed of fine clay, silt, sand, and gravel, are primarily derived from the weathering of the Himalayan crystalline and metasedimentary rocks and peninsular lithologies (Rahaman et al., 2012; Singh et al., 2008). The Himalayan rivers drain granite-gneisses, calc-silicates, metamorphosed carbonates, black shales, and meta-sedimentary rocks (Rahaman et al., 2012), whereas peninsular rivers traverse the Deccan basalts, the Vindhyan sedimentary rocks, the Bundelkhand crystalline complexes and granites (Singh et al., 2008). The tributaries of the Hooghly River: the Rupnarayan, the Damodar, and the Ajay, drain primarily through the acidic rocks of the Archean Gneissic complex, sandstones, shales, the Gondwana coal measures and lateritic alluvium (Mondal et al., 2018; Sarkar et al., 2004).

3. Materials and Methods

Water and sediment samples were collected from the Hooghly River between Kolkata and Nischindipur (~90 km downstream of Kolkata; Fig. 1b) during 2012-2020, covering periods of contrasting discharges, pre-monsoon (PrM: January to June), monsoon (M: July-September), and post-monsoon (PoM: October-December). The sediment samples include both suspended and surface sediments. In addition, groundwater samples from areas adjacent to the Hooghly River and domestic and industrial effluent water samples from the Kolkata metropolitan area were collected in 2013. The detailed sampling and processing protocols are provided in the Supplementary materials (Section S1).

Temperature, pH, total dissolved solids (TDS), salinity, conductivity, and dissolved oxygen (DO) were measured in situ using portable multi-electrode probes (Eutech PCSTestr 35 and Hach HQ40d). Concentrations of HCO_3^- and CO_3^{2-} were measured by manual acid-base titration in the

field and by an auto titrator (Metrohm 916 Ti-touch) in the lab. The major anion and cation concentrations in water samples were measured using an ion chromatograph (Thermo Scientific Dionex ICS-5000) facility at the Indian Institute of Science Education and Research (IISER) Kolkata. The Re concentrations in water and sediment samples were determined by isotope dilution. Concentrations of Al, Na, K, Ca, and Cs in sediment samples were measured using a quadrupole ICP-MS (Thermo Scientific X series 2) facility at IISER Kolkata. Silicon concentrations in surface sediments were determined by X-ray fluorescence (Bruker S8 Tiger WD). OC concentrations and $\delta^{13}C_{org}$ in sediment samples were measured using isotope-ratio mass spectrometry (IRMS) facilities at Physical Research Laboratory (PRL), Ahmedabad and IISER Pune. Radiocarbon measurements (expressed as percent modern carbon; pMC) of sediment samples were performed using the Accelerator Mass Spectrometry (AMS) facility at the Inter-University Accelerator Centre (IUAC), Delhi. The details of measurements, and their accuracy and precision, are provided in the Supplementary materials (section S2).

4. Results

The dissolved Re concentrations ($[Re]_{diss}$) of the Hooghly River varied from 5.0 to 12.9 pmol/kg across sampling periods. These measured $[Re]_{diss}$ values are bracketed by those reported for the Ganga River at Allahabad (13.3 pM; Rahaman et al., 2012) and near Hardinge Bridge in Bangladesh (3.9 pM; Miller et al., 2011). Also, PoM samples of this study (October 2012) bracket $[Re]_{diss}$ value (5.2±0.3 pmol/kg) determined for the Hooghly River freshwater for December 2006 (Rahaman and Singh, 2010).

The PrM periods (January to June) are generally characterized by higher $[Re]_{diss}$ values (9.2 to 12.9 pmol/kg) whereas, in PoM periods (October to December), $[Re]_{diss}$ values were the lowest (5.0 to 6.2 pmol/kg; Supplementary materials Fig. SF1). Seasonal variation was also

reported by Dalai et al. (2002) in the upper reaches of the Ganga River at Rishikesh, where $[Re]_{diss}$ varied from 5.3 pmol/kg in M, 6.7 pmol/kg in PoM, to 7.9 pmol/kg in PrM period. No distinct spatial trend of $[Re]_{diss}$ was observed in the stretch between Rishikesh (in the foothills of the Himalayas) and Kulpi, ~90 km downstream of Kolkata.

The Re concentrations are in the range of ~95-1240 pg/g in the SPM and ~85-160 pg/g in the surface sediments (Supplementary materials Fig. SF2). With the exception of two samples of January 2020 collection, the measured [Re] values in the SPM and surface sediments are ~3-10 folds lower than those reported for the Ganga River SPM (583-631 pg/g) at Allahabad and Farakka (Chakrapani et al., 2002) and the Ganga River surface sediments at Rajmahal (353-1195 pg/g; Rahaman et al., 2012), but are comparable to the lower end of the [Re] variability reported (114-797 pg/g) in the Ganga River surface sediments at Rajshahi in Bangladesh (Pierson-Wickmann et al., 2000).

5. Discussion

5.1. Influence of solute-particle interaction on sedimentary Re abundances

While Re is considered to be highly mobile owing to its ability to form perrhenate (ReO_4^-) complexes in oxygenated aqueous medium (Brookins, 1986; Colodner et al., 1993; Koide et al., 1986), a few recent studies alluded to its particle-reactive nature (Danish et al., 2021; Tanaka et al., 2019). In the Hooghly River, Re/Al ratios exhibit significant positive correlation with Si/Al ratios in surface sediments (Fig. 2a). Given that Si/Al ratio is an indicator of hydrodynamic sorting and associated mineral or size fractionation (Lupker et al., 2012b), the Re/Al-Si/Al positive correlation (Fig. 2a) indicates that Re is mainly associated with coarse-sized fractions. The Si/Al ratios are also a result of variable weathering intensity as evident from an inverse correlation of

Si/Al ratios with Chemical Index of Alteration (CIA; Nesbitt and Young, 1982; Fig. 2b) and a positive correlation with Na/Al ratios (Fig. 2a). Therefore, we infer that weathering intensity exerts a more dominant control on the Re abundances in the surface sediments than processes such as ion-exchange and adsorption. A lack of any covariation trends between Re/Al and Cs/Al ratios (Supplementary materials Fig. SF3) further corroborates the above inference, given that Cs^{+}, being a large ion, is preferentially adsorbed onto secondary phases in soil and sedimentary systems (Fuller et al., 2014; Kabata-Pendias and Pendias, 2001; Park et al., 2019). Our observation of a lack of particle-reactive behaviour of Re is consistent with thermodynamic model calculations of perrhenate ions (Brookins, 1986; Nikolaychuk, 2022), which predict its stability over a wide pH range (0-14) in oxygenated environments (E_h > 0.3). While the influence of solute-particle interaction appears insignificant in regulating Re abundances in the Hooghly River sediments, we recognize the need for further studies to assess Re partitioning in soil and sediment systems under variable conditions of pH, E_h, and relative significance of relevant phases (e.g., exchangeable, organic and oxyhydroxides).

5.2. Sources of dissolved Re

Rhenium concentrations range from ~10 to 50 pg/g in silicate lithologies (Dalai et al., 2002; Pearson et al., 2004), whereas a larger range of values (0 to 225 pg/g) was reported for the Lesser Himalayan carbonate rocks (Dalai et al., 2002). The estimates of average [Re] in UCC vary from 198 pg/g (Peucker-Ehrenbrink and Jahn, 2001) to 500 pg/g (Taylor and McLennan, 1985). In contrast, reported [Re] values in organic-rich sediments such as black shales, a minor lithology, are typically higher and exhibit variation by orders of magnitude, in the range of 60 pg/g to 2.9 μg/g (Ghazi et al., 2024 and references therein; Peucker-Ehrenbrink and Hannigan, 2000; Singh et al., 1999). The sulfide minerals such as molybdenite (MoS_2), pyrite (FeS_2), chalcopyrite ($CuFeS_2$),

and rheniite (ReS_2) also contain elevated amounts of Re, ranging from 0.022 ng/g to 1000 μg/g (Miller et al., 2011 and references therein; Sinclair et al., 2016). Among sulfide minerals, rheniite is a rare mineral that contains Re as a primary constituent. In contrast, molybdenite is the most significant and abundant source of Re, with concentrations as high as 1000 μg/g (Sinclair et al., 2016). In the following, we evaluate the significance of major and minor lithologies in supplying dissolved Re to the Hooghly River.

5.2.1. Anthropogenic contributions

In the post-industrial periods, Re distributions in surface waters, groundwaters, and soils are known to be influenced by anthropogenic activities such as the mining of porphyry copper (Cu) deposits (Barton et al., 2020; John et al., 2017; Miller et al., 2011), petroleum industries (Rahaman and Singh, 2010; Wang et al., 2024), combustion of fossil fuel (Chappaz et al., 2008; Colodner et al., 1995), and emissions from smelting industries (Chappaz et al., 2008; Rahaman et al., 2012). Elevated $[Re]_{diss}$ values were also reported in the Indian Rivers, including the lower reaches of the Yamuna (Agra and Allahabad), Godavari, Narmada, Ghod, Gomti, Sabarmati, and Mahi, which are impacted by both mining and industrial activities (Rahaman et al., 2012). Globally, the average riverine [Re] (~16 pmol/L) is estimated to have increased by ~50-60% relative to the pre-industrial period values of ~10 to 11 pmol/L (Ghazi et al., 2024; Miller et al., 2011) due to anthropogenic activities.

The Hooghly River flows through densely populated and industrialized regions (Kolkata, Howrah, Haldia, Batanagar, Budge-Budge), receiving substantial urban and industrial effluents. These effluent waters exhibit 11.2 to 13.0 pmol/kg of [Re], which is comparable to the upper limit

of riverine $[Re]_{diss}$ (~12.9 pmol/kg). Anthropogenic Re contribution ($[Re]_{anth}$ (%)) was determined as:

$$[Re]_{anth}\ (\%) = \left(\frac{[Re]^{avg}_{effluent} \times f_{effluent}}{[Re]_{river}}\right) \times 100 \qquad (1)$$

where $[R]^{avg}_{effluent}$ represents average [Re] in effluent water (11.9±0.9 pmol/kg), $[Re]_{river}$ is Re concentration in river water samples, and $f_{effluent}$ is the fraction of effluent water contribution to the river water discharge. The urban and industrial effluent water discharge to the Hooghly River increased from 1154×10^6 L/day in the year 2005 (Sadhuram et al., 2005) to 7495×10^6 L/day in 2020 (Central Pollution Control Board, 2020; Rajan et al., 2023), comprising maximum of ~8% of river water during lean flow (in February) and ~1-3% during the monsoon period (July-September). Using the $f_{effluent}$ value in eq. (1), it is estimated that up to ~10% of dissolved Re during lean flow periods (January to February) is supplied by effluent discharge, whereas the maximum contribution of ~5% in the monsoon period cannot be resolved considering the analytical uncertainty. We consider these estimates likely represent the upper limit of anthropogenic Re contributions to the Hooghly River given that the $[Re]_{diss}$ of the Hooghly River remained similar during monsoon periods over a span of eight years (2012 to 2019). Our evaluation, therefore, indicates that anthropogenic sources can supply ~10% of river water Re during lean-flow periods, whereas their impact is negligible during peak-flow conditions.

5.2.2. Major lithologies

The variation trends of Mg/Na vs Ca/Na ratios provide valuable information on weathering contributions from major lithologies (silicates and carbonates), as well as from rainwater and groundwater (Gaillardet et al., 1999). In a plot of molar ratios of Ca/Na and Mg/Na (Supplementary materials Fig. SF4), most of the river water data fall along the mixing trend between silicate and

carbonate end-member compositions, indicating that weathering of these lithologies drives the major element composition of the river water. The dissolved Re concentrations, however, show inverse correlation with [HCO_3^-] during PrM and combined M and PoM period (Fig. 3a) and with ΣCations* during PrM period (ΣCations*=[Na*]+[K]+[Mg]+[Ca], where Na* is the cyclic input corrected Na and is computed as [Na]-[Cl]; Fig. 3b). Furthermore, Re/ΣCations* ratios in the Hooghly River waters are higher than those Re/ΣCations ratios reported for the Himalayan silicate and carbonate minerals (Dalai et al., 2002) by more than two orders of magnitude (Supplementary materials Table ST1). These observations, together, support the inference that major lithologies make only a minor contribution to the dissolved Re budget of the Hooghly River.

5.2.3. Sulfide minerals

The [Re]-[SO_4] positive correlation in the river waters (Colodner et al., 1993; Dalai et al., 2002; Miller et al., 2011; Rahaman et al., 2012) is interpreted as evidence of the supply of dissolved Re via oxidation of sulfide minerals, particularly when sulfide minerals are associated with Re-enriched black shale. The sulfuric acid produced by the chemical weathering of sulfide minerals reacts with black shales and associated minerals, releasing constituent elements and resulting in the observed [Re]-[SO_4] correlation. In the Hooghly River, plots of $[Re]_{diss}$ vs [SO_4] and [SO_4]/ΣAnions (Fig. 4a and b) exhibit a scattered distribution rather than well-defined linear trends. These observations most likely result from mixing of variable contributions from cyclic sources (rain and evaporites) and saline groundwater, which are characterized by low Re/Cl and Re/SO_4 ratios, with inputs from sulfide minerals with higher Re/S and Re/Cl ratios. The mixing of these distinct sources is clearly illustrated in a plot of Re/Cl vs SO_4/Cl ratios (Fig. 4c), which exhibits a strong positive correlation. Groundwater samples demonstrate rather lower Re/Cl and Re/SO_4 ratios, indicating that they contribute only a minor fraction to the dissolved Re load.

In Fig. 4d, we observe that Re/Cl and SO_4/Cl ratios exhibit a strong positive correlation with ΣCations/[Cl]. These observations, together with the variation trends of [Re]/[Cl] with [SO_4]/[Cl] (Fig. 4c), imply that sulfide minerals associated with major lithologies are dispersed throughout the catchment and contribute at least partially to the dissolved Re budgets. Therefore, dissolved Re concentrations in the Hooghly River waters, after being deconvolved for cyclic and groundwater sources, can be explained by the weathering of major lithologies and trace minerals and phases associated with them. As major lithologies are not dominant sources of Re to the rivers (section 5.2.2), the dominant source(s) of Re are inferred to be phases such as sulfides and OC associated with them. It is noteworthy that in the variation plots of [Re]/[Cl] and [SO_4]/[Cl] vs ΣCations/[Cl], these ratios of the groundwater are much lower than the values in the river waters (Fig. 4d). Therefore, we infer that Re abundances in the Hooghly waters are unlikely to be significantly impacted by groundwater contributions.

5.2.4. Rhenium contribution from petrogenic carbon

As discussed earlier, silicate and carbonate rocks are not significant sources of dissolved Re. The negative correlations between Re/Al ratio and CIA in SPM and surface sediments (Fig. 5) are indicative of Re loss during progressive weathering. Furthermore, the positive correlation observed between Re/Al and OC/Al ratios in SPM and surface sediments (Fig. 6a) indicates that Re and OC share common sources or pathways or both. However, a scattered distribution is observed in a plot of OC/Al vs CIA (Supplementary materials Fig. SF5). In addition, OC/Al ratios exhibit a nearly threefold variation across a narrow CIA range of 3-4 units in several surface sediment samples. Together, these observations are consistent with the presence of two OC pools: one associated with bedrocks that varies as a function of CIA (OC_{petro}), and another that is independent of lithological influence (OC_{bio}). The inferred presence of two distinct pools of

organic matter in the river sediments is further supported by an inverse correlation observed between Re/Al ratios and $\delta^{13}C_{org}$ (Fig. 6b). Since OC constitutes both OC_{petro} and OC_{bio} components, the $\delta^{13}C_{org}$ values may reflect their relative abundance if they have substantial isotopic contrast. We evaluate the relative importance of these two organic pools in regulating the distribution of Re in sediments before employing dissolved [Re] as a proxy for OC_{petro} oxidation within the basin.

Earlier studies on the Ganga River (Galy et al., 2008a) and the Mackenzie River (Hilton et al., 2015) sediments show that at lower degree of weathering, sediments have higher contents of OC_{petro}, and lower $\delta^{13}C_{org}$ values. The observation of a positive $\delta^{13}C_{org}$-CIA correlation for the Hooghly River sediments (Fig. 6c) is consistent with less weathered sediments being characterized by higher OC_{petro} and lower $\delta^{13}C_{org}$ values. In addition, $\delta^{13}C_{org}$-CIA variation trend also implies a greater loss of OC_{petro} at higher intensity of weathering. The observed variation trends (Fig. 6b and c) also support the notion that higher Re concentrations in the sediments are primarily due to OC_{petro}. Such an inference is consistent with the knowledge that Re contents are higher in OC_{petro} (Zhang et al., 2024) and in marine organic-rich sediments, such as black shales, than in terrestrial organic-rich phases such as soil and coal (Baioumy et al., 2011). The Re/OC ratios of the SPM and surface sediments are, therefore, regulated by a mixture of OC_{bio} with a lower Re/OC ratio and OC_{petro} with a higher Re/OC ratio (Hilton et al., 2014; Horan et al., 2019). It is observed that Re/OC ratios of the SPM are inversely correlated with CIA (Fig. 6d). This observation could result from (i) a decrease in the fraction of OC_{petro} due to weathering or (ii) preferential release of Re relative to OC_{petro} during weathering (Grant et al., 2025; Jaffe et al., 2002; Zhang et al., 2024) or both. However, some surface sediments, characterized by a nearly three-fold variation in OC/Al (Supplementary materials Fig. SF5), show about two-fold variability in Re/OC ratios for a narrow

change (3-4 units) of CIA values (Fig. 6d). While the cause of such observations cannot be ascertained based on available data, it is likely that these sediment samples have variable abundances of OC_{bio}, which can result from either variable supply from the catchment or different degrees of degradation of OC_{bio} or both.

5.3. Apportionment of dissolved Re sources

We first separate the cyclic source contribution (precipitation, evaporites, and saline groundwater) to dissolved Re from that from the non-cyclic sources (anthropogenic, silicates, carbonates, sulfides, and OC_{petro}), before determining Re supply from OC_{petro} oxidation. The detailed approaches of source apportionments and calculations are provided in the Supplementary materials (section S7).

Our calculations (Supplementary materials eq. s1-5) show that oxidative weathering of OC_{petro} is the dominant contributor, accounting for 74-92% of dissolved Re in the Hooghly River and up to 97% of Re in the Ganga River and its tributaries (unpublished data). In contrast, Re contributions from weathering of silicate rocks and sulfide minerals are minor. Silicate weathering contributes <1% whereas sulfide oxidation accounts for typically 3-11% of dissolved Re in the GHR system. No significant variation in fraction of dissolved Re contribution from OC_{petro} oxidation was observed between the upper and lower reaches of the Ganga River and between peak and lean discharge periods.

The observations and calculations bring out several important features of OC_{petro} oxidation and its impact on the dissolved Re in the GHR system: (i) OC_{petro} contributions to dissolved Re are broadly similar for various rivers of the GHR system and (ii) oxidation of OC_{petro} is the dominant

365 source of dissolved Re to GHR system, whose catchment areas are characterized by widely varying
366 topography, hydrology, lithology and climate.

367 **5.4. The CO_2 release flux due to OC_{petro} oxidation**

368 Although the CO_2 release flux due to oxidative weathering can be determined from the
369 dissolved Re flux associated with OC_{petro} oxidation and the Re/OC ratio in bedrocks (Dalai et al.,
370 2002), this approach assumes congruent release of OC_{petro} and Re during oxidative weathering. In
371 this study, we estimate the carbon release ($J_{OCpetro\ oxidation}$) following the approach of Horan et al.
372 (2019), which accounts for the fraction of oxidation-resistant graphitized OC_{petro}.

373 $$J_{OCpetro\ oxidation} = J_{diss\ Re} \times \left[\frac{OC}{Re}\right]_{petro} \times f_{OCpetro}^{Re} \times (1-f_{graphite}) \quad (2)$$

374 where $J_{diss\ Re}$ is the dissolved Re yield (mol/km^2/yr), $[OC/Re]_{petro}$ is the OC/Re ratio of OC_{petro} in
375 the catchment lithology, $f_{OCpetro}^{Re}$ is the fraction of dissolved Re derived from the OC_{petro} oxidation,
376 and $f_{graphite}$ represents the fraction of graphitic OC_{petro}. The annual dissolved Re fluxes were
377 determined using mean annual discharge and discharge-weighted $[Re]_{diss}$ of the Hooghly River
378 (Supplementary materials section S8-9). The $[OC]_{petro}$ values, determined from the total OC and
379 radiocarbon content (pMC), are 0.11±0.07 wt.% in SPM and 0.07±0.02 wt.% in surface sediments,
380 corresponding to 12-23% and 10-32% of [OC], respectively (Supplementary materials section
381 S10).

382 To estimate $[Re/OC]_{petro}$, we use a plot of Re/OC ratios vs mass fraction of OC_{petro} in
383 sediments. The observed positive correlation (Fig. 7) reinforces the inference that the Re/OC ratio
384 in OC_{petro} is higher than that in OC_{bio} (Horan et al., 2019). At 100% OC_{petro}, the regression of data
385 in Fig. 7 provides an estimate of $[Re/OC]_{petro}$, 1.37±0.20×10^{-7} g/g. This value falls within the range

of Re/OC ratios reported for Lesser Himalayan black shales ((0.7-66) $\times 10^{-7}$ g/g) and is comparable to the values (0.3-8.4) $\times 10^{-7}$ g/g) reported for global river basins (Supplementary materials Table ST2).

In the Ganga River sediments in Bangladesh, Galy et al. (2008a) observed that OC_{petro} present is predominantly graphitic, accounting for 40±10% of total OC_{petro}. Therefore, we substitute a value of 0.4±0.1 for $f_{graphite}$, $f_{OCpetro}^{Re}$ values of 0.74-0.92 as determined above, and $[Re/OC]_{petro}$ of 1.37±0.20$\times 10^{-7}$ (g/g) in eq. (2), and determine that the CO_2 release yield due to OC_{petro} oxidation is (3.5-4.4)$\times 10^4$ mol/km^2/yr in the GHR catchment. The CO_2 release yield peaks at (4.3-7.0)$\times 10^3$ mol/km^2/month during the monsoon, whereas the lowest yield of (1.5-1.6)$\times 10^3$ mol/km^2/month occurs during the lean-flow period in February. Notably, we observe that CO_2 release via oxidative weathering is comparable to, or even exceeds, CO_2 consumption by silicate weathering during high discharge periods, whereas CO_2 consumption by silicate weathering predominates during low discharge periods (Fig. 8). These observations suggest that, during high-discharge periods, oxidative weathering of OC_{petro} may be efficient due to a combination of higher reactivity of OC_{petro} than silicates (Chang and Berner, 1999; Scheingross et al., 2019) and greater exposure of OC_{petro} driven by enhanced physical erosion in the GHR catchment (Roy and Sinha, 2017; Samanta and Dalai, 2016). Previous studies have also highlighted the role of physical erosion in the export and oxidation of OC_{petro} in river catchments (Galy et al., 2015; Hilton et al., 2014; Horan et al., 2017).

5.5. Drivers of OC_{petro} oxidation: Physical erosion and beyond

We now evaluate the role of erosion in the oxidation-driven CO_2 release across the entire GHR catchment as well as the lower Ganga basin in Bangladesh. While the elevated physical

erosion rates in the Himalayan catchment result mainly from high relief and tectonic activity, monsoonal rainfall and associated runoff sustain high physical erosion in the lower basin (Khan et al., 2018; Roy and Sinha, 2017; Samanta and Dalai, 2016). The coupled impact of tectonics and monsoonal climate is evident in a strong positive correlation between annual SPM flux and water discharge in catchments from the high altitude region in the Himalayas to the flat lands in the lower reaches of India and Bangladesh (Samanta and Dalai, 2016).

The combined data for the global river basins and the Ganga River basin, when plotted on a log-log plot of CO_2 release yield vs sediment yield (Fig. 9a), exhibit a power-law relationship that is indistinguishable from global data alone (Zondervan et al., 2023). The broad agreement of the global data with that from the Ganga River basin reinforces the notion that a power-law model adequately captures most of the variability in OC_{petro} yields as a function of physical erosion on a global scale. Additionally, our results show two distinct power-law trends for mountainous and floodplain catchments (Fig. 9b), the former with a lower scaling constant ($a = 1.98 \pm 11.0 \times 10^{-11}$) and unusually higher exponent ($b = 4.65 \pm 0.69$), and the latter with a much higher scaling constant ($a = 1094 \pm 1357$), and lower exponent ($b = 0.74 \pm 0.13$). Note, however, the Yamuna and Chambal data are the distinct outliers. While available data are insufficient to provide a clear explanation for this observation, it may result from basin-specific variability in $[Re/OC]_{petro}$, which can differ by more than an order of magnitude ($(0.3\text{-}8.4) \times 10^{-7}$ g/g, Supplementary materials Table ST2), or from variation in the style and rate of $[OC]_{petro}$ oxidation between catchments, particularly between mountain and plain regions, or from a combination of both these factors. It is noteworthy to mention that the Chambal River catchment is confined exclusively to the peninsular flat region, whereas the other rivers drain the Himalayas in their upper reaches.

The observation of a lower scaling constant and a unrealistically higher exponent, as mentioned above, in river catchments with high erosion yields (>2000 t/km^2/yr) in the mountains (Fig. 9b) calls for an explanation. Such a relationship implies that $[OC]_{petro}$ oxidation yields are negligible at lower end of the observed range of high erosion yields in these mountainous catchments. We propose that in catchments with steep topography and high erosion yields, a certain fraction of OC_{petro} undergoes limited to negligible oxidation. This apparent lack of oxidation is unlikely to result from slower $[OC]_{petro}$ oxidation kinetics, as $[OC]_{petro}$ oxidation is not considered rate-limiting under high erosion conditions (Hemingway et al., 2018; Hilton et al., 2014). Instead, as discussed hereafter, one or more additional mechanisms contribute to insignificant $[OC]_{petro}$ oxidation in the mountainous region. (i) Lack of soil weathering and priming of OC_{petro}: Several studies have demonstrated that the initiation of $[OC]_{petro}$ oxidation can be stimulated by labile organic matter through a process known as "priming" (Chen et al., 2022; Lien et al., 2025). Hemingway et al. (2018) further showed that microbial activity within the soil weathering zone drives $[OC]_{petro}$ oxidation in the mountainous regions of Taiwan. An important finding from their work is that $[OC]_{petro}$ oxidation may be inhibited when large volumes of sediment are rapidly mobilized by major earthquakes or typhoons, which trigger bedrock landslides. In such cases, although catchment-averaged erosion rates increase, the efficiency of $[OC]_{petro}$ oxidation may decrease for sediments that are not exposed to soil weathering. (ii) Competition for available oxygen: While $[OC]_{petro}$ oxidation can occur spontaneously in the vadose zone (Bolton et al., 2006; Ghazi et al., 2025; Hilton et al., 2021), it must compete for available oxygen with more rapidly oxidizing phases, such as sulfide minerals and OC_{bio} (Bolton et al., 2006; Gu et al., 2020; Hemingway et al., 2018). Although how OC_{petro} oxidation is impacted in such a scenario is unclear, it is likely its efficiency is hindered when the oxygen diffusion to the deeper level is limited.

A plot of OC_{petro} oxidation vs erosion yields exhibits a significant positive linear correlation for mountainous catchment in the GHR basin (r=0.99, Supplementary materials Fig. SF8). The x-intercept (2324 t/km^2/yr) in this plot represents the average sediment yield transported from the mountainous region of the GHR basin associated with no OC_{petro} oxidation. After subtracting this value from the total sediment yield of each mountainous catchment, the CO_2 release and the sediment yield data define a power law with an exponent indistinguishable from 1.0 (Fig. 9b). It is noteworthy that, even after applying the above correction in the sediment yield, the exponent remains 35% higher than that derived from data for floodplain catchments. This indicates that, for a given erosion yield, higher carbon release yield is achieved in mountainous region than in floodplains. Existing studies indicate that enhanced oxidation of OC_{petro} is driven by from both rapid physical erosion and greater exposure of bedrocks in the steep terrains, as well as longer sediment residence times in floodplains (Dellinger et al., 2023; Hilton et al., 2014). Our observation that carbon release yields are higher in the mountainous catchments than in the floodplains of the GHR basin indicates that erosion-driven exposure of OC_{petro} in the mountainous region likely exerts a stronger control on OC_{petro} oxidation than prolonged sediment residence times in the floodplains. Alternatively, additional mechanisms may enhance the efficiency of OC_{petro} oxidation in steep terrains. Deeper fluid penetration and the associated increase in the water saturation depth in steeper mountainous terrains has been proposed to promote increased and deeper diffusion of oxygen from the atmosphere into solution, and thereby enhancing oxidative weathering (Stolze et al., 2026).

Collectively, the results and observations discussed above indicate that oxidative weathering is governed by distinct controls and mechanisms, and that its relationship with physical erosion, as well as sediment and fluid transport, differs between mountainous regions and

floodplains. Further investigation of river basins encompassing both mountainous catchments and floodplains is required to better constrain the competing controls on OC_{petro} oxidation in these contrasting environments.

5.6. Net atmospheric CO_2 balance in the GHR catchment

The net CO_2 balance in a catchment reflects the combined effects of weathering of silicate and carbonate rocks, oxidation of OC_{petro} and burial of OC_{bio}. Among these processes, silicate weathering and OC_{bio} burial act as atmospheric CO_2 sinks. The OC_{bio} burial yield (J_{OCbio_burial}) in the GHR catchment was estimated following the approach of Hilton et al. (2008) as follows:

$$J_{OCbio\_burial}=J_{SPM} \times [OC]_{bio} \times E_{OC\text{-}burial} \quad (3)$$

where J_{SPM} denotes SPM yield (t/km^2/yr), and $E_{OC\text{-}burial}$ is the efficiency of organic carbon burial (%). Using an average $[OC]_{bio}$ (=[OC]-$[OC]_{petro}$) of 0.57±0.12 wt.%, a burial efficiency of 30-100% reported for the Bengal Basin (Galy et al., 2007) and a SPM flux of 328×10^6 t/yr (Abbas and Subramanian, 1984), we estimate an OC_{bio} burial flux of $(0.5\text{-}1.6)\times10^5$ mol/km^2/yr. In comparison, CO_2 release from OC_{petro} oxidation is $(3.5\text{-}4.4)\times10^4$ mol/km^2/yr, offsetting 22-90% of the CO_2 sequestered by OC_{bio} burial. Such a result highlights the significance of OC_{petro} oxidation and its quantification in the long-term carbon cycle.

The net atmospheric CO_2 balance (J_{net}) in the GHR catchment is expressed as:

$$J_{net} = J_{OCpetro\ oxidation} - J_{CO2\_silicate\ weathering} - J_{OCbio\_burial} \quad (4)$$

where $J_{CO2\_silicate\ weathering}$ represents CO_2 consumption due to silicate weathering. Our estimates suggest that the CO_2 release due to OC_{petro} oxidation ($4.2\pm1.0\times10^4$ mol/km^2/yr) is nearly offset by the CO_2 drawdown via silicate weathering ($4.2\pm0.6\times10^4$ mol/km^2/yr). In contrast, CO_2

497 sequestration through OC_{bio} burial ($1.1\pm0.5\times10^5$ mol/km^2/yr) is nearly three times greater than
498 either of these fluxes. As a result, the GHR catchment functions as a net atmospheric CO_2 sink
499 (Fig. 10), primarily driven by the high sediment flux and subsequent OC_{bio} burial. Additionally,
500 our findings are in agreement with the study of (Galy et al., 2008a), which demonstrated that in
501 the Ganga River basin in Bangladesh, CO_2 drawdown flux via silicate weathering is nearly similar
502 to that of CO_2 release via OC_{petro} oxidation, whereas CO_2 sequestration due to OC_{bio} burial was
503 approximately five times greater than the CO_2 release from OC_{petro} oxidation. We acknowledge
504 that our estimates provide an upper bound on net CO_2 sequestration, as our approach (eq. 4) does
505 not account for CO_2 release from sulfuric acid-mediated carbonate weathering.

506 **6. Conclusions**

507 This study, by integrating data on major and trace elements, dissolved and particulate Re,
508 $\delta^{13}C_{org}$ and pMC, presents the first comprehensive assessment of OC_{petro} oxidation and net carbon
509 balance in the GHR basin in India. The main findings are summarized below.

510 Although the dominant lithologies largely control the major-element composition of river
511 waters, they contribute little to the dissolved Re budget. Chloride-normalized [Re]-[SO_4] plots
512 indicate that rainwater, groundwater, and evaporites are minor sources of dissolved Re. Our
513 analysis also suggests that anthropogenic inputs contribute up to 10% of dissolved Re during low-
514 flow conditions but are negligible during peak flow periods.

515 Mass balance calculations indicate that OC_{petro} oxidation is the dominant contributor to the
516 dissolved Re budgets, accounting for up to 97% of the dissolved Re in the GHR system. The
517 estimates of CO_2 release due to OC_{petro} oxidation in the GHR basin show distinct seasonal
518 variability, with higher values during peak flow periods than during lean flow periods. Notably,

519 CO_2 emissions from OC_{petro} oxidation equal or exceed CO_2 consumption by silicate weathering
520 during high discharge periods, whereas the reverse phenomenon occurs during low discharge
521 periods.

522 In the Ganga River basin, CO_2 release from OC_{petro} oxidation scales with sediment yield
523 according to a power-law relationship. This pattern is consistent with observations from global
524 river catchments and reinforces the view that physical erosion exerts a first-order control over
525 OC_{petro} oxidation. In the mountainous regions of the GHR basin where erosion yields exceed 2000
526 $t/km^2/yr$, a fraction of OC_{petro} experiences limited to negligible oxidation, likely due to a lack of
527 priming effect and rapid bedrock transport that bypasses soil weathering. Nevertheless, the OC_{petro}
528 release yield in the mountainous region exceeds that in the floodplains at comparable physical
529 erosion yields. The higher OC_{petro} release yields in the steeper mountainous terrains result from the
530 combined effects of accelerated physical erosion, greater bedrock exposure, and enhanced fluid
531 penetration and oxygen diffusion into the fluid-sediment system.

532 Although CO_2 released from OC_{petro} oxidation is nearly balanced by CO_2 consumption by
533 silicate weathering in the GHR basin, OC_{bio} burial exceeds both these processes, resulting in a net
534 negative carbon budget. Thus, despite substantial CO_2 emissions from OC_{petro} oxidation, the GHR
535 catchment functions as a net carbon sink, primarily due to the high efficiency of OC_{bio} burial
536 facilitated by elevated sediment transport.

537

538

539

540

541

CRediT authorship contribution statement

RS: Conceptualization, Data curation, Formal analysis, Investigation, Methodology, Project administration, Software, Validation, Visualization, Writing - original draft, Writing - review & editing. **TKD:** Conceptualization, Data curation, Funding acquisition, Methodology, Project administration, Resources, Supervision, Validation, Visualization, Writing - original draft, and Writing - review & editing. **KM:** Resources, Methodology, Formal analysis, Validation, Data Curation. **PK:** Resources, Methodology, Formal analysis, Validation, Data Curation. **DK**: Methodology, Formal analysis, Validation, Data Curation. **SK**: Resources, Methodology, Formal analysis, Validation, Data Curation.

Acknowledgements

RS thanks the Council of Scientific and Industrial Research (CSIR), India, for providing a research fellowship (Award no.: 07/921(0332)/2020-EMR-I). TKD also acknowledges the financial support from IISER Kolkata through the ARF grant. We thank Dr. Santosh Ch. Das for assistance with ICP-MS analysis, and Dr. Rajveer Sharma and Ms. Leema Saikia for their help with radiocarbon analysis.

Appendix A. Supplementary Materials

Supplementary materials include the following:

Section S1: Details of sample collection and processing

Section S2: Details of analytical method

Section S3: Concentrations of Re in the Hooghly River water and sediment samples

Section S4: Variation of [Re]/[Al] with [Cs]/[Al] in the Hooghly River sediments

Section S5: Variation of [Mg]/[Na] vs. [Ca]/[Na] ratios in the Hooghly River water

Section S6: Variation of [OC]/[Al] ratios with CIA in the Hooghly River sediments

Section S7: Fraction of dissolved Re contribution from non-cyclic sources

Section S8: Estimation of monthly water discharge of the Hooghly River for the years 2013-2020

Section S9: Estimation of dissolved Re flux

Section S10: Estimation of $[OC]_{petro}$ in the Hooghly River sediments

Section S11: Estimation of CO_2 consumption due to silicate weathering in the Ganga–Hooghly River catchment

Section S12: The CO_2 release due to OC_{petro} oxidation as a function of erosion yield in the mountainous catchments of the Ganga–Hooghly River basin

Section S13: Supplementary Tables (Table ST1-ST2)

References

Abbas, N., Subramanian, V., 1984. Erosion and sediment transport in the Ganges river basin (India). Journal of Hydrology 69(1), 173-182. https://doi.org/10.1016/0022-1694(84)90162-8.

Allison, M.A., Khan, S.R., Goodbred, S.L., Kuehl, S.A., 2003. Stratigraphic evolution of the late Holocene Ganges–Brahmaputra lower delta plain. Sedimentary Geology 155(3), 317-342. https://doi.org/10.1016/S0037-0738(02)00185-9.

Baioumy, H.M., Eglinton, L.B., Peucker-Ehrenbrink, B., 2011. Rhenium–osmium isotope and platinum group element systematics of marine vs. non-marine organic-rich sediments and coals from Egypt. Chemical Geology 285(1), 70-81. https://doi.org/10.1016/j.chemgeo.2011.02.026.

Barton, I.F., Rathkopf, C.A., Barton, M.D., 2020. Rhenium in Molybdenite: a Database Approach to Identifying Geochemical Controls on the Distribution of a Critical Element. Mining, Metallurgy & Exploration 37(1), 21-37. https://doi.org/10.1007/s42461-019-00145-0.

Bolton, E.W., Berner, R.A., Petsch, S.T., 2006. The Weathering of Sedimentary Organic Matter as a Control on Atmospheric O2: II. Theoretical Modeling. American Journal of Science 306(8), 575-615. https://doi.org/10.2475/08.2006.01.

Bouchez, J., Beyssac, O., Galy, V., Gaillardet, J., France-Lanord, C., Maurice, L., Moreira-Turcq, P., 2010. Oxidation of petrogenic organic carbon in the Amazon floodplain as a source of atmospheric CO2. Geology 38(3), 255-258. 10.1130/G30608.1.

Brookins, D.G., 1986. Rhenium as analog for fissiogenic technetium: Eh-pH diagram (25°C, 1 bar) constraints. Applied Geochemistry 1(4), 513-517. https://doi.org/10.1016/0883-2927(86)90056-9.

Central Pollution Control Board, B., 2020. Status of post-monsoon 2020 monitored drains discharging into River Ganga and its tributaries. Central Pollution Control Board, New Delhi, India. https://cpcb.nic.in/ngrba/Identified_drains_postmonsoon-2020.pdf

Chakrapani, G.J., Gaillardet, J., Dupre, B., Allegre, C.J., 2002. Osmium isotopic compositions in Ganga river sediments. Current Science 83(10), 1253-1255. https://www.jstor.org/stable/24106480.

Chang, S., Berner, R.A., 1999. Coal weathering and the geochemical carbon cycle. Geochimica et Cosmochimica Acta 63(19), 3301-3310. https://doi.org/10.1016/S0016-7037(99)00252-5.

Chappaz, A., Gobeil, C., Tessier, A., 2008. Sequestration mechanisms and anthropogenic inputs of rhenium in sediments from Eastern Canada lakes. Geochimica et Cosmochimica Acta 72(24), 6027-6036. https://doi.org/10.1016/j.gca.2008.10.003.

Chen, X., Lin, J., Wang, P., Zhang, S., Liu, D., Zhu, B., 2022. Resistant soil carbon is more vulnerable to priming effect than active soil carbon. Soil Biology and Biochemistry 168, 108619. https://doi.org/10.1016/j.soilbio.2022.108619.

Colodner, D., Edmond, J., Boyle, E., 1995. Rhenium in the Black Sea: comparison with molybdenum and uranium. Earth and Planetary Science Letters 131(1), 1-15. https://doi.org/10.1016/0012-821X(95)00010-A.

Colodner, D., Sachs, J., Ravizza, G., Turekian, K., Edmond, J., Boyle, E., 1993. The geochemical cycle of rhenium: a reconnaissance. Earth and Planetary Science Letters 117(1), 205-221. https://doi.org/10.1016/0012-821X(93)90127-U.

Crusius, J., Calvert, S., Pedersen, T., Sage, D., 1996. Rhenium and molybdenum enrichments in sediments as indicators of oxic, suboxic and sulfidic conditions of deposition. Earth and Planetary Science Letters 145(1), 65-78. https://doi.org/10.1016/S0012-821X(96)00204-X.

Dalai, T.K., Singh, S.K., Trivedi, J.R., Krishnaswami, S., 2002. Dissolved rhenium in the Yamuna river system and the Ganga in the Himalaya: role of black shale weathering on the budgets of Re,

Os, and U in rivers and CO2 in the atmosphere. Geochimica et Cosmochimica Acta 66(1), 29-43. https://doi.org/10.1016/S0016-7037(01)00747-5.
Danish, M., Tripathy, G.R., Mitra, S., Rout, R.K., Raskar, S., 2021. Non-conservative removal of dissolved rhenium from a coastal lagoon: Clay adsorption versus biological uptake. Chemical Geology 580, 120378. https://doi.org/10.1016/j.chemgeo.2021.120378.
Dellinger, M., Hilton, R.G., Baronas, J.J., Torres, M.A., Burt, E.I., Clark, K.E., Galy, V., Ccahuana Quispe, A.J., West, A.J., 2023. High rates of rock organic carbon oxidation sustained as Andean sediment transits the Amazon foreland-floodplain. Proceedings of the National Academy of Sciences 120(39), e2306343120. https://doi.org/10.1073/pnas.2306343120.
Fuller, A.J., Shaw, S., Peacock, C.L., Trivedi, D., Small, J.S., Abrahamsen, L.G., Burke, I.T., 2014. Ionic strength and pH dependent multi-site sorption of Cs onto a micaceous aquifer sediment. Applied Geochemistry 40, 32-42. https://doi.org/10.1016/j.apgeochem.2013.10.017.
Gaillardet, J., Dupré, B., Louvat, P., Allègre, C.J., 1999. Global silicate weathering and CO2 consumption rates deduced from the chemistry of large rivers. Chemical Geology 159(1), 3-30. https://doi.org/10.1016/S0009-2541(99)00031-5.
Galy, V., Beyssac, O., France-Lanord, C., Eglinton, T., 2008a. Recycling of Graphite During Himalayan Erosion: A Geological Stabilization of Carbon in the Crust. Science 322(5903), 943-945. https://doi.org/10.1126/science.1161408.
Galy, V., France-Lanord, C., Beyssac, O., Faure, P., Kudrass, H., Palhol, F., 2007. Efficient organic carbon burial in the Bengal fan sustained by the Himalayan erosional system. Nature 450(7168), 407-410. https://doi.org/10.1038/nature06273.
Galy, V., France-Lanord, C., Lartiges, B., 2008b. Loading and fate of particulate organic carbon from the Himalaya to the Ganga–Brahmaputra delta. Geochimica et Cosmochimica Acta 72(7), 1767-1787. https://doi.org/10.1016/j.gca.2008.01.027.
Galy, V., Peucker-Ehrenbrink, B., Eglinton, T., 2015. Global carbon export from the terrestrial biosphere controlled by erosion. Nature 521(7551), 204-207. https://doi.org/10.1038/nature14400.
Ghazi, L., Grant, K.E., Chappaz, A., Danish, M., Peucker-Ehrenbrink, B., Pett-Ridge, J.C., 2024. The Global Biogeochemical Cycle of Rhenium. Global Biogeochemical Cycles 38(10), e2024GB008254. https://doi.org/10.1029/2024GB008254.
Grant, K.E., Dellinger, M., Dickson, A.J., Ogric, M., Horan, K., Petsch, S., Hilton, R.G., 2025. Validating the rhenium proxy for rock organic carbon oxidation using weathering profiles. Chemical Geology 671, 122464. https://doi.org/10.1016/j.chemgeo.2024.122464.
Gu, X., Rempe, D.M., Dietrich, W.E., West, A.J., Lin, T.-C., Jin, L., Brantley, S.L., 2020. Chemical reactions, porosity, and microfracturing in shale during weathering: The effect of erosion rate. Geochimica et Cosmochimica Acta 269, 63-100. https://doi.org/10.1016/j.gca.2019.09.044.
Hemingway, J.D., Hilton, R.G., Hovius, N., Eglinton, T.I., Haghipour, N., Wacker, L., Chen, M.-C., Galy, V.V., 2018. Microbial oxidation of lithospheric organic carbon in rapidly eroding tropical mountain soils. Science 360(6385), 209-212. https://doi.org/10.1126/science.aao6463.
Hilton, R.G., Gaillardet, J., Calmels, D., Birck, J.-L., 2014. Geological respiration of a mountain belt revealed by the trace element rhenium. Earth and Planetary Science Letters 403, 27-36. https://doi.org/10.1016/j.epsl.2014.06.021.
Hilton, R.G., Galy, A., Hovius, N., 2008. Riverine particulate organic carbon from an active mountain belt: Importance of landslides. Global Biogeochemical Cycles 22(1). https://doi.org/10.1029/2006GB002905.

Hilton, R.G., Galy, V., Gaillardet, J., Dellinger, M., Bryant, C., O'Regan, M., Gröcke, D.R., Coxall, H., Bouchez, J., Calmels, D., 2015. Erosion of organic carbon in the Arctic as a geological carbon dioxide sink. Nature 524(7563), 84-87. https://doi.org/10.1038/nature14653.
Horan, K., Hilton, R.G., Dellinger, M., Tipper, E., Galy, V., Calmels, D., Selby, D., Gaillardet, J., Ottley, C.J., Parsons, D.R., Burton, K.W., 2019. Carbon dioxide emissions by rock organic carbon oxidation and the net geochemical carbon budget of the Mackenzie River Basin. American Journal of Science 319(6), 473-499. https://doi.org/10.2475/06.2019.02.
Horan, K., Hilton, R.G., Selby, D., Ottley, C.J., Grocke, D.R., Hicks, M., Burton, K.W., 2017. Mountain glaciation drives rapid oxidation of rock-bound organic carbon. Sci Adv 3(10), e1701107. https://doi.org/10.1126/sciadv.1701107.
Jaffe, L.A., Peucker-Ehrenbrink, B., Petsch, S.T., 2002. Mobility of rhenium, platinum group elements and organic carbon during black shale weathering. Earth and Planetary Science Letters 198(3), 339-353. https://doi.org/10.1016/S0012-821X(02)00526-5.
John, D., Seal Ii, R.R., Polyak, D.E., 2017. Rhenium, in: Schulz, K., DeYoung, Jr., Seal, I.I.R.R., Bradley, D. (Eds.), Professional Paper. Reston, VA, p. 62. https://doi.org/10.3133/pp1802P
Kabata-Pendias, A., Pendias, H., 2001. Soil constituents, in: Kabata-Pendias, A., Pendias, H. (Eds.), Trace elements in soils and plants. CRC Press, pp. 43-64.
Khan, S., Sinha, R., Whitehead, P., Sarkar, S., Jin, L., Futter, M.N., 2018. Flows and sediment dynamics in the Ganga River under present and future climate scenarios. Hydrological Sciences Journal 63(5), 763-782. https://doi.org/10.1080/02626667.2018.1447113.
Koide, M., Hodge, V.F., Yang, J.S., Stallard, M., Goldberg, E.G., Calhoun, J., Bertine, K.K., 1986. Some comparative marine chemistries of rhenium, gold, silver and molybdenum. Applied Geochemistry 1(6), 705-714. https://doi.org/10.1016/0883-2927(86)90092-2.
Lien, W.-Y., Chen, C.-T., Lee, Y.-H., Su, C.-C., Wang, P.-L., Lin, L.-H., 2025. Two-stage oxidation of petrogenic organic carbon in a rapidly exhuming small mountainous catchment. Communications Earth & Environment 6(1), 45. https://doi.org/10.1038/s43247-025-02015-8.
Lupker, M., France-Lanord, C., Galy, V., Lavé, J., Gaillardet, J., Gajurel, A.P., Guilmette, C., Rahman, M., Singh, S.K., Sinha, R., 2012. Predominant floodplain over mountain weathering of Himalayan sediments (Ganga basin). Geochimica et Cosmochimica Acta 84, 410-432. https://doi.org/10.1016/j.gca.2012.02.001.
Lupker, M., France-Lanord, C., Lavé, J., Bouchez, J., Galy, V., Métivier, F., Gaillardet, J., Lartiges, B., Mugnier, J.-L., 2011. A Rouse-based method to integrate the chemical composition of river sediments: Application to the Ganga basin. Journal of Geophysical Research: Earth Surface 116(F4). https://doi.org/10.1029/2010JF001947.
Miller, C.A., Peucker-Ehrenbrink, B., Walker, B.D., Marcantonio, F., 2011. Re-assessing the surface cycling of molybdenum and rhenium. Geochimica et Cosmochimica Acta 75(22), 7146-7179. https://doi.org/10.1016/j.gca.2011.09.005.
Mondal, G.C., Singh, A.K., Singh, T.B., 2018. Damodar River Basin: Storehouse of Indian Coal, in: Singh, D.S. (Ed.) The Indian Rivers: Scientific and Socio-economic Aspects. Springer Singapore, Singapore, pp. 259-272. doi.org/https://doi.org/10.1007/978-981-10-2984-4_21.
Mukhopadhyay, A., Acharyya, R., Habel, M., Pal, I., Pramanick, N., Hati, J.P., Sanyal, M.K., Ghosh, T., 2023. Upstream River Erosion vis-a-vis Sediments Variability in Hugli Estuary, India: A Geospatial Approach. Water 15(7), 1285. https://doi.org/10.3390/w15071285.
Nesbitt, H.W., Young, G.M., 1982. Early Proterozoic climates and plate motions inferred from major element chemistry of lutites. Nature 299(5885), 715-717. https://doi.org/10.1038/299715a0.

Nikolaychuk, P.A., 2022. The potential—pH diagram for rhenium. Chemical Thermodynamics and Thermal Analysis 7, 100068. https://doi.org/10.1016/j.ctta.2022.100068.
Park, S.-M., Alessi, D.S., Baek, K., 2019. Selective adsorption and irreversible fixation behavior of cesium onto 2:1 layered clay mineral: A mini review. Journal of Hazardous Materials 369, 569-576. https://doi.org/10.1016/j.jhazmat.2019.02.061.
Pearson, D.G., Irvine, G.J., Ionov, D.A., Boyd, F.R., Dreibus, G.E., 2004. Re–Os isotope systematics and platinum group element fractionation during mantle melt extraction: a study of massif and xenolith peridotite suites. Chemical Geology 208(1), 29-59. https://doi.org/10.1016/j.chemgeo.2004.04.005.
Peucker-Ehrenbrink, B., Hannigan, R.E., 2000. Effects of black shale weathering on the mobility of rhenium and platinum group elements. Geology 28(5), 475-478. https://doi.org/10.1130/0091-7613(2000)28<475:EOBSWO>2.0.CO;2.
Peucker-Ehrenbrink, B., Jahn, B.-m., 2001. Rhenium-osmium isotope systematics and platinum group element concentrations: Loess and the upper continental crust. Geochemistry, Geophysics, Geosystems 2(10). https://doi.org/10.1029/2001GC000172.
Pierson-Wickmann, A.-C., Reisberg, L., France-Lanord, C., 2000. The Os isotopic composition of Himalayan river bedloads and bedrocks: importance of black shales. Earth and Planetary Science Letters 176(2), 203-218. https://doi.org/10.1016/S0012-821X(00)00003-0.
Rahaman, W., Singh, S.K., 2010. Rhenium in rivers and estuaries of India: Sources, transport and behaviour. Marine Chemistry 118(1), 1-10. https://doi.org/10.1016/j.marchem.2009.09.008.
Rahaman, W., Singh, S.K., Shukla, A.D., 2012. Rhenium in Indian rivers: Sources, fluxes, and contribution to oceanic budget. Geochemistry, Geophysics, Geosystems 13(8). https://doi.org/10.1029/2012GC004083.
Rajan, K., Khudsar, F.A., Kumar, R., 2023. Spatio-temporal patterns of microplastic contamination in surface waters of Hooghly River Estuary: Causes and consequences. Regional Studies in Marine Science 65, 103111. https://doi.org/10.1016/j.rsma.2023.103111.
Roy, N.G., Sinha, R., 2017. Linking hydrology and sediment dynamics of large alluvial rivers to landscape diversity in the Ganga dispersal system, India. Earth Surface Processes and Landforms 42(7), 1078-1091. https://doi.org/10.1002/esp.4074.
Rudra, K., 2014. Changing river courses in the western part of the Ganga–Brahmaputra delta. Geomorphology 227, 87-100. https://doi.org/10.1016/j.geomorph.2014.05.013.
Sadhuram, Y., Sarma, V.V., Murthy, T.V.R., Rao, B.P., 2005. Seasonal variability of physico-chemical characteristics of the Haldia channel of Hooghly estuary, India. Journal of Earth System Science 114(1), 37-49. https://doi.org/10.1007/BF02702007.
Samanta, S., Dalai, T.K., 2016. Dissolved and particulate Barium in the Ganga (Hooghly) River estuary, India: Solute-particle interactions and the enhanced dissolved flux to the oceans. Geochimica et Cosmochimica Acta 195, 1-28. https://doi.org/10.1016/j.gca.2016.09.005.
Sarkar, S.K., Frančišković-Bilinski, S., Bhattacharya, A., Saha, M., Bilinski, H., 2004. Levels of elements in the surficial estuarine sediments of the Hugli River, northeast India and their environmental implications. Environment International 30(8), 1089-1098. https://doi.org/10.1016/j.envint.2004.06.005.
Scheingross, J.S., Hovius, N., Dellinger, M., Hilton, R.G., Repasch, M., Sachse, D., Gröcke, D.R., Vieth-Hillebrand, A., Turowski, J.M., 2019. Preservation of organic carbon during active fluvial transport and particle abrasion. Geology 47(10), 958-962. https://doi.org/10.1130/G46442.1.
Schlitzer, R., 2021. Ocean Data View (Version 5.5.2). https://odv.awi.de.

Sinclair, W.D., Jonasson, I.R., Kirkham, R.V., Soregaroli, A.E., 2016. Rhenium in Canadian mineral deposits. Geological Survey of Canada, Ottawa, Canada. publications.gc.ca/pub?id=9.956396&sl=0.

Singh, S.K., Rai, S.K., Krishnaswami, S., 2008. Sr and Nd isotopes in river sediments from the Ganga Basin: Sediment provenance and spatial variability in physical erosion. Journal of Geophysical Research: Earth Surface 113(F3). https://doi.org/10.1029/2007JF000909.

Singh, S.K., Trivedi, J.R., Krishnaswami, S., 1999. Re-Os isotope systematics in black shales from the Lesser Himalaya: their chronology and role in the 187Os/188Os evolution of seawater. Geochimica et Cosmochimica Acta 63(16), 2381-2392. https://doi.org/10.1016/S0016-7037(99)00201-X.

Stolze, L., Dwivedi, D., Steefel, C., Molins, S., Dong, W., Beutler, C., Newman, A., Williams, K., 2026. Model-Based Interpretation of Solute Exports and Carbon Partitioning During Shale Weathering in a Mountainous Hillslope. 62(3), e2025WR041597. https://doi.org/10.1029/2025WR041597.

Tanaka, K., Kozai, N., Ohnuki, T., Grambow, B., 2019. Study on coordination structure of Re adsorbed on Mg–Al layered double hydroxide using X-ray absorption fine structure. Journal of Porous Materials 26(2), 505-511. https://doi.org/10.1007/s10934-018-0634-z.

Taylor, S.R., McLennan, S.M., 1985. The continental crust: Its composition and evolution. Blackwell Scientific Publications, Malden, MA.

Wang, Y., Li, S., Xu, P., Wang, H., Chen, Y., Chen, J., 2024. Rapid and significant perturbations on the global geochemical cycle of rhenium by human activities ----- A case study in Yangtze River basin. Applied Geochemistry 162, 105912. https://doi.org/10.1016/j.apgeochem.2024.105912.

Zhang, Y., Wang, J., Qu, Y., Zhu, C., Jin, Z., 2024. Mobility of rhenium and selenium during chemical weathering and their implication for petrogenic organic carbon oxidation. Science China Earth Sciences 67(3), 740-750. https://doi.org/10.1007/s11430-023-1244-5.

Zondervan, J.R., Hilton, R.G., Dellinger, M., Clubb, F.J., Roylands, T., Ogrič, M., 2023. Rock organic carbon oxidation CO2 release offsets silicate weathering sink. Nature 623(7986), 329-333. https://doi.org/10.1038/s41586-023-06581-9.

Figures

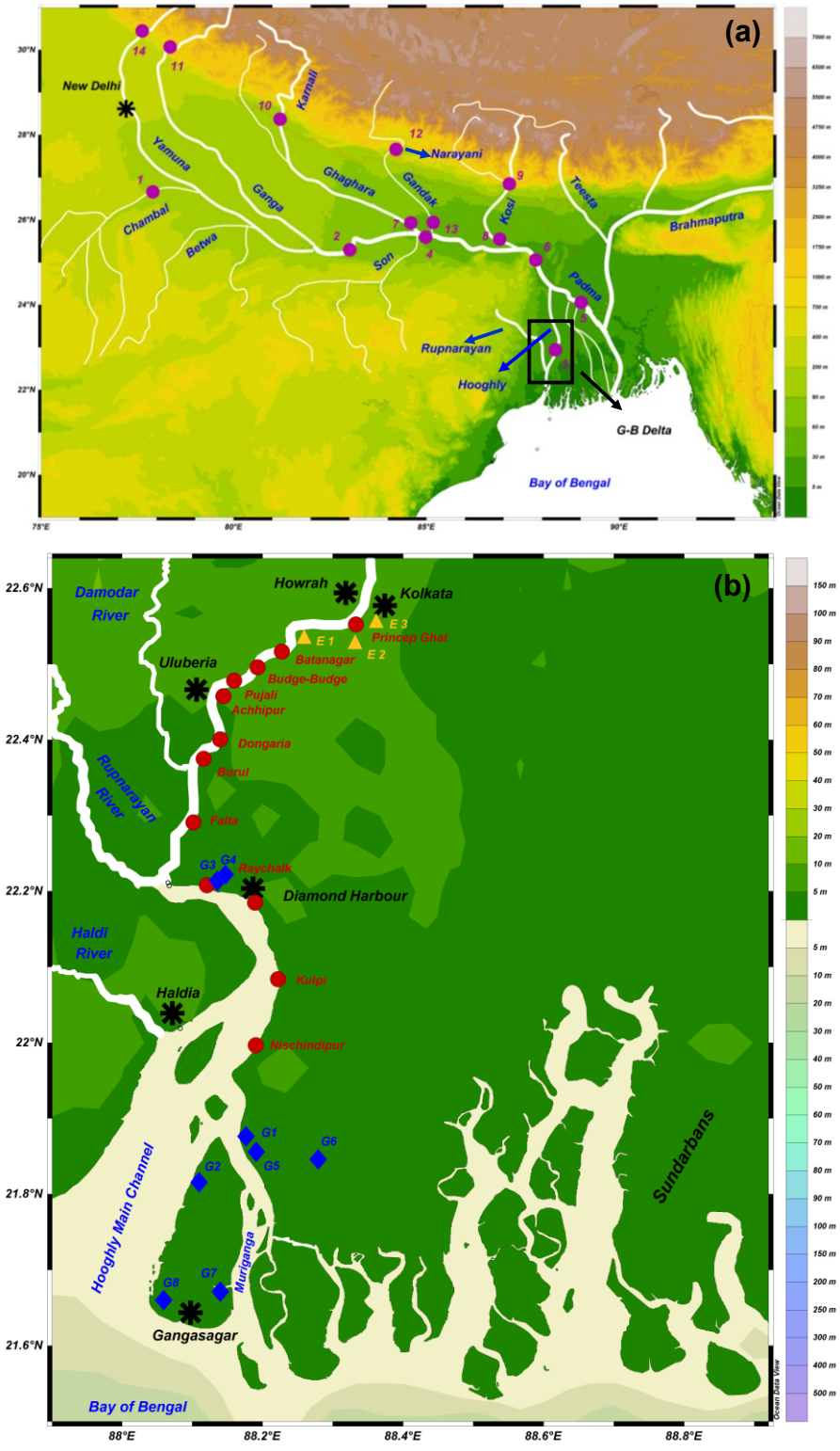

Fig. 1. (a) The Ganga-Hooghly River (GHR) system and its tributaries draining the Himalayas and the peninsular India. The Ganga–Brahmaputra (G-B) delta system is also shown. The rectangle

represents the study area (not to the scale) of the Hooghly River system in the lower reaches of the GHR basin. Locations where dissolved Re concentrations ($[Re]_{diss}$) are used in this study (pink circles) to determine OC_{petro} oxidation are numbered: (1) Dhaulpur, (2) Varanasi, (3) Kolkata, (4) Patna, (5) Hardinge bridge, (6) Rajmahal (7) Revilganj, (8) Dhumarighat, (9) Chatara, (10) Kothiaghat, (11) Rishikesh, (12) Narayangaht, (13) Hazipur and (14) Batamandi. Except for Kolkata (this study), $[Re]_{diss}$ data are sourced from Miller et al. (2011), Rahaman et al. (2012) and Dalai et al. (2002). **(b)** The sampling locations for river water (red circle), groundwater (blue diamond), and effluent water (yellow triangle). Black stars represent major towns or cities. Location and depth of groundwater sampling: (G1) Kakdwip-61 m, (G2) Sapkhali-67 m, (G3) Raychalk-46 m, (G4) Raychalk-34 m, (G5) Kakdwip-37 m, (G6) Kakdwip-15 m, (G7) Chemaguri-76 m, (G8) Lighthouse-61 m. Industrial and urban effluent water sample location: (E1) Garden Reach, (E2) Majerhat, and (E3) Babughat. The color-coded elevation values are in meters above sea level (Fig. 1a, b). Ocean Data View (ODV) software was used for making digital elevation map (Schlitzer, 2021, https://odv.awi.de).

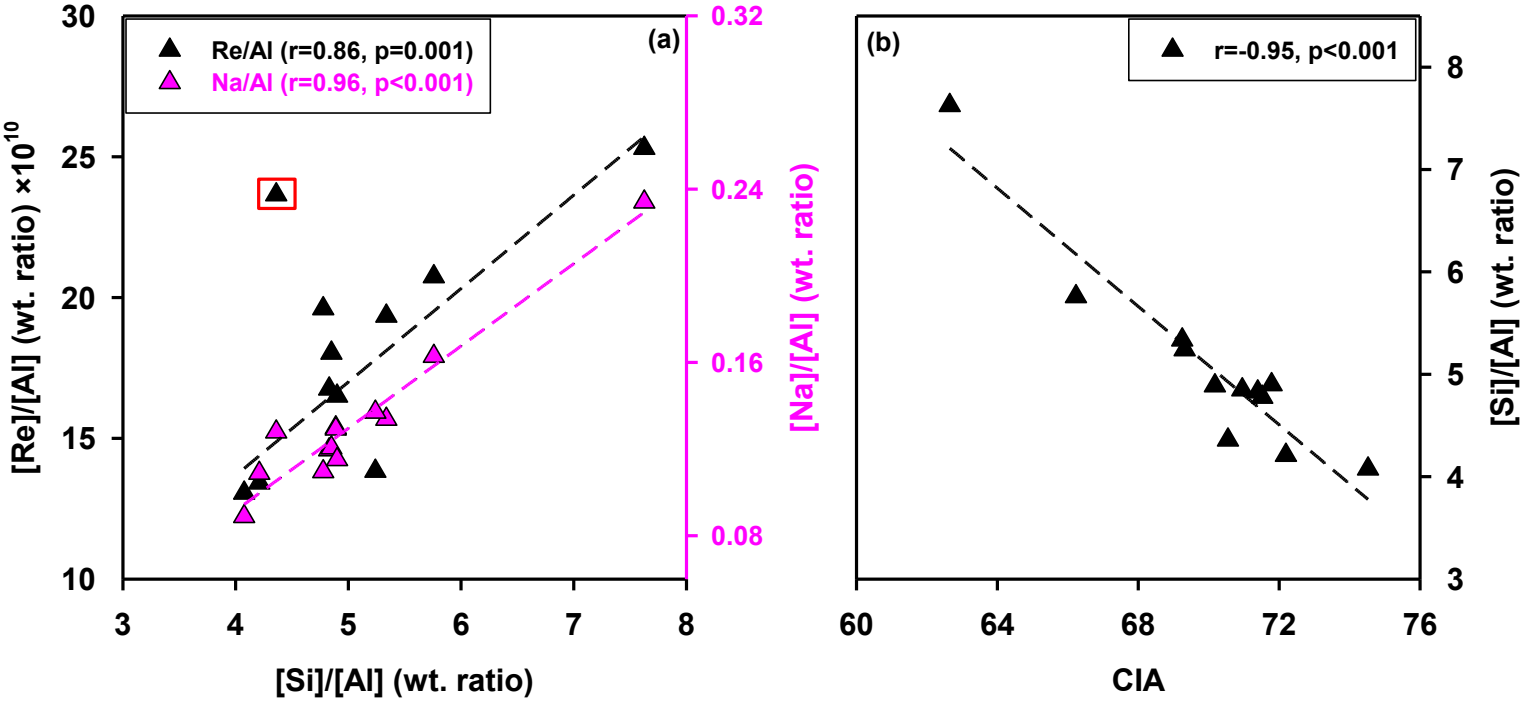

Fig. 2. Variation of **(a)** [Re]/[Al] and [Na]/[Al] as a function of [Si]/[Al] and (**b**) [Si]/[Al] with CIA in the Hooghly River surface sediments. The positive correlations observed for [Re]/[Al] and [Na]/[Al] with [Si]/[Al] ratios, in conjunction with an inverse correlation between [Si]/[Al] and CIA, is indicative of lower Re concentrations in sediments that have undergone higher degree of weathering, characterized by lower [Na]/[Al] and [Si]/[Al] ratios and higher CIA values. Trends of linear regression are shown as dashed lines. One outlier (marked in red in box) was excluded from the regression.

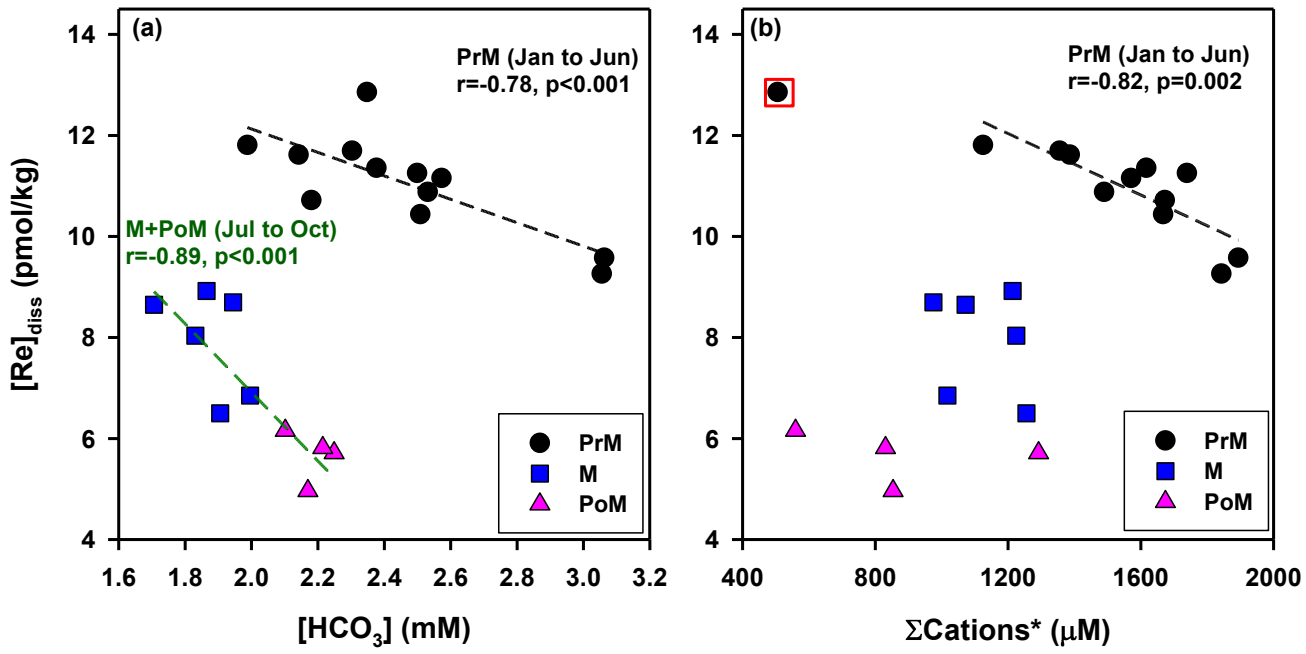

Fig. 3. Variation of $[Re]_{diss}$ with **(a)** $[HCO_3]$ and **(b)** ΣCations* in the Hooghly River. The inverse correlations suggest that weathering of major lithologies is not a driver of dissolved Re concentrations. Trends of linear regression are shown as dashed lines. One outlier (in the box) was excluded from the regression.

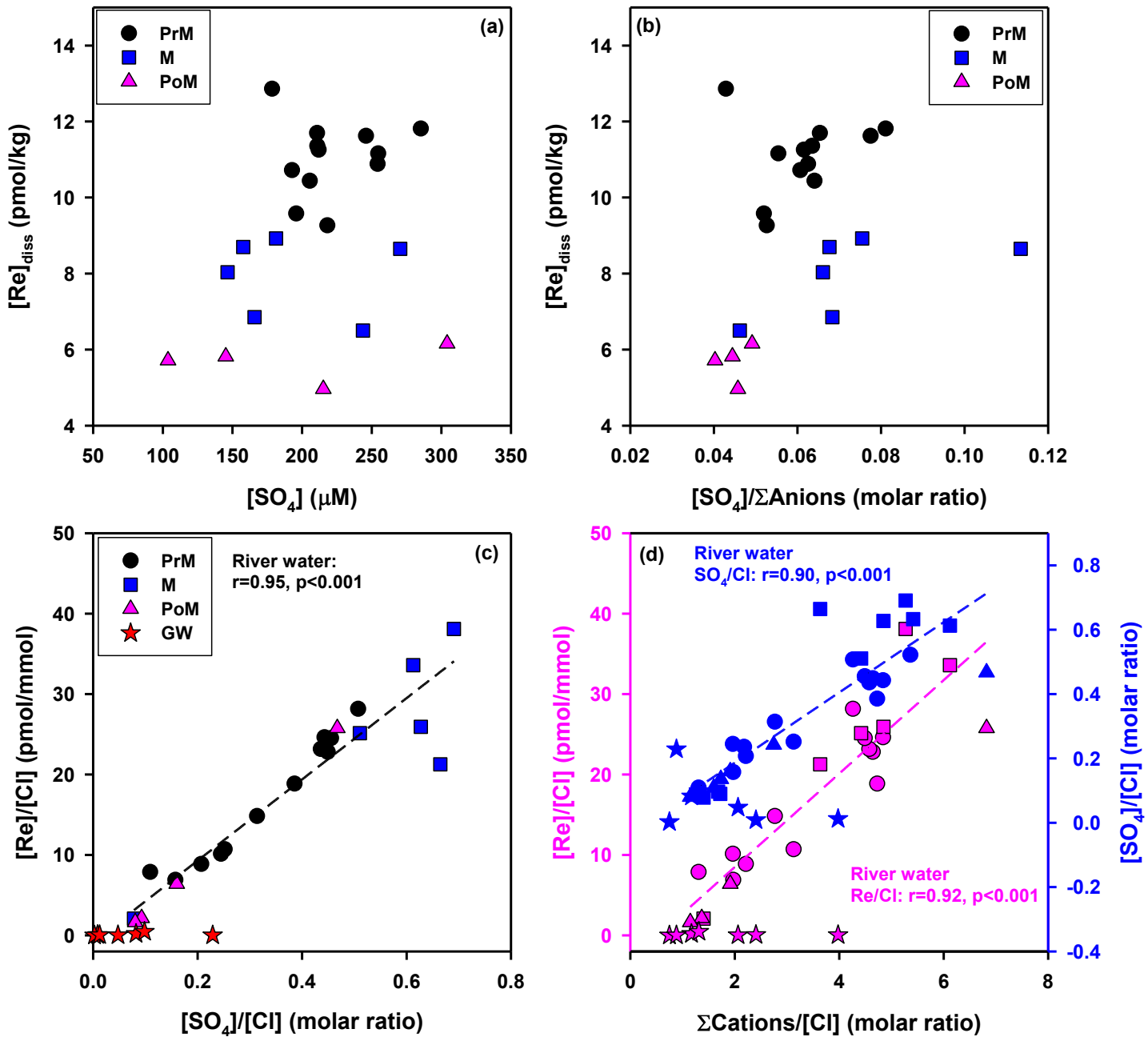

Fig. 4. Variation of **(a)** $[Re]_{diss}$ with $[SO_4]$, **(b)** of $[Re]_{diss}$ with $[SO_4]/\Sigma$Anions, **(c)** of Re]/[Cl] with $[SO_4]/[Cl]$, and **(d)** of [Re]/[Cl] and $[SO_4]/[Cl]$ with ΣCations/[Cl] for the Hooghly River water (pre-monsoon: circles; monsoon: squares; post-monsoon: triangles) and groundwater (stars). The absence of a significant correlation in (a) and (b) indicates that dissolved Re and SO_4 are derived from multiple sources in variable relative proportions. The strong positive linear relationships of [Re]/[Cl] with both $[SO_4]/[Cl]$ and ΣCations/[Cl] suggest mixing between Re-poor sources (e.g., rainwater and evaporites) and Re-rich sources (e.g., sulfides and petrogenic organic carbon). Lower [Re]/[Cl] and $[SO_4]/[Cl]$ ratios in groundwater indicate that groundwater is not a significant contributor of dissolved Re. The overall positive correlation of [Re]/[Cl] and $[SO_4]/[Cl]$ with ΣCations/[Cl] implies an association of Re-rich phases and sulfide minerals with major lithologies,

whereas increased scatter at higher [SO_4]/[Cl] and ΣCations/[Cl] values points to an additional non-sulfide source contributing to elevated dissolved Re in the river.

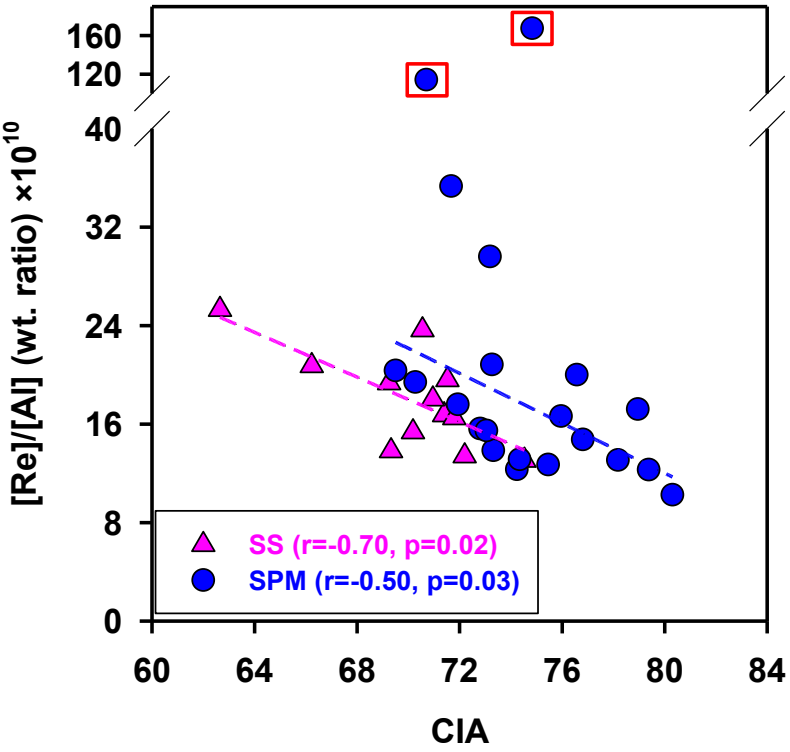

Fig. 5. Variation of [Re]/[Al] ratios with CIA in the Hooghly River sediments (SPM: suspended particulate matter, SS: surface sediment). The inverse correlations indicate that Re is released from rocks during progressive weathering. Trends of linear regression are shown as dashed lines. Two outliers (in the box) were excluded from the regression.

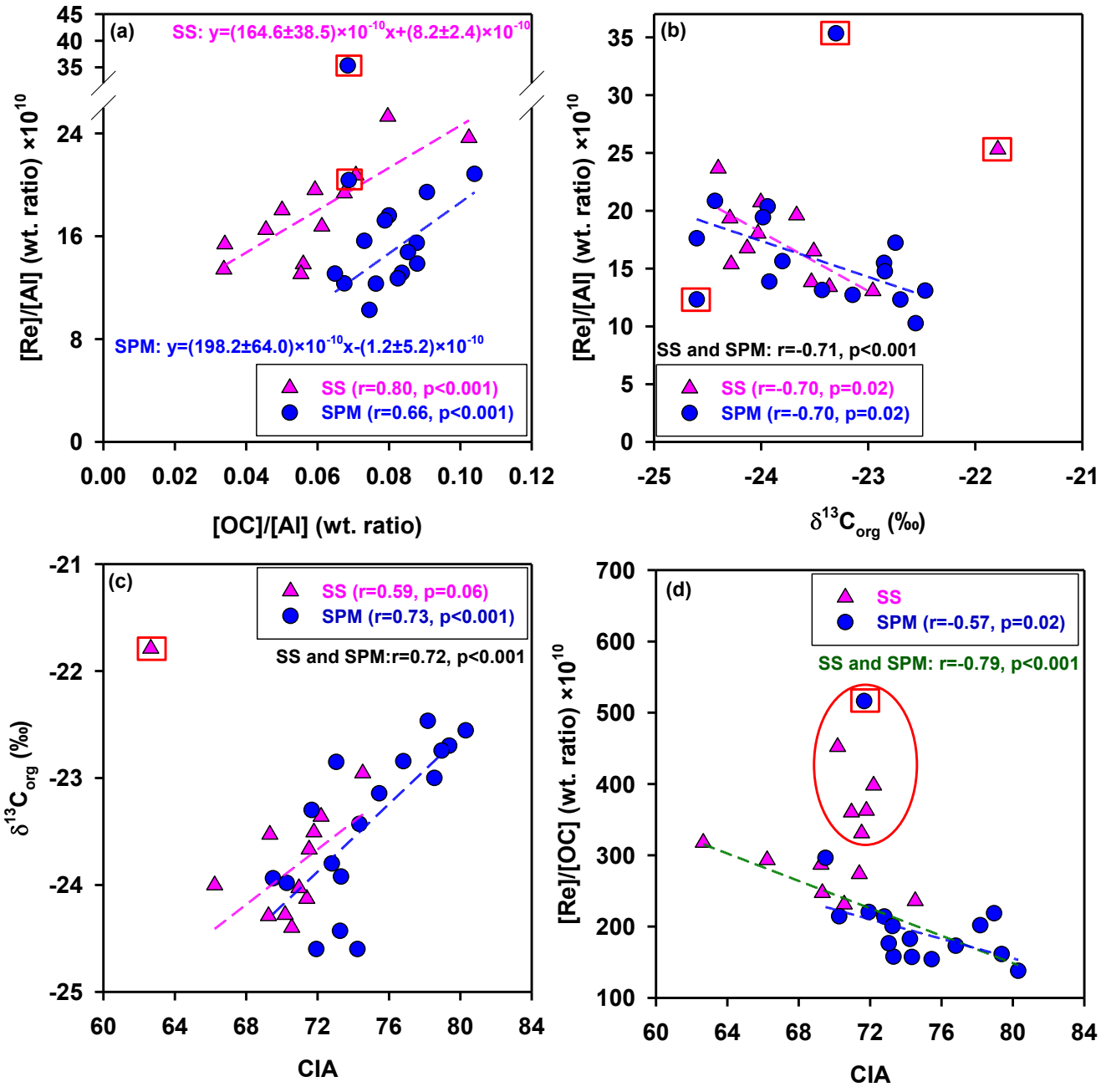

Fig. 6. Variation of **(a)** [Re]/[Al] ratios with [OC]/[Al] ratios, **(b)** of [Re]/[Al] ratios with $\delta^{13}C_{org}$ **(c)** of $\delta^{13}C_{org}$ with CIA and **(d)** of [Re/OC] ratios with CIA in the Hooghly River sediments (SPM: suspended particulate matter, SS: surface sediment). The positive correlations in (a) indicate that Re and OC share common sources and/or pathways. The inverse correlations in (b) and positive correlations in (c) indicate that Re is associated with OC with low $\delta^{13}C_{org}$ values (OC_{petro}). These trends together suggest a progressive loss of OC_{petro} with increasing weathering intensity, as evident from lower $\delta^{13}C_{org}$ values in the less weathered sediments having higher OC_{petro} fractions. The inverse correlation in (d) can be explained by either preferential loss of Re over OC_{petro} or decreasing fractions of OC_{petro} (i.e. increasing proportions of Re-poor OC_{bio}) during progressive

weathering. Trends of linear regression are shown as dashed lines. Outliers (in the box) were excluded from the regression analysis. The green dashed line (d) represents the linear regression for SS and SPM, excluding data points in the ellipse. These outliers (in ellipse), characterized by a larger variability of [Re]/[OC] over a narrow range of CIA values, are likely a result of dominant influence of variable OC_{bio} abundances (see section 5.2.4).

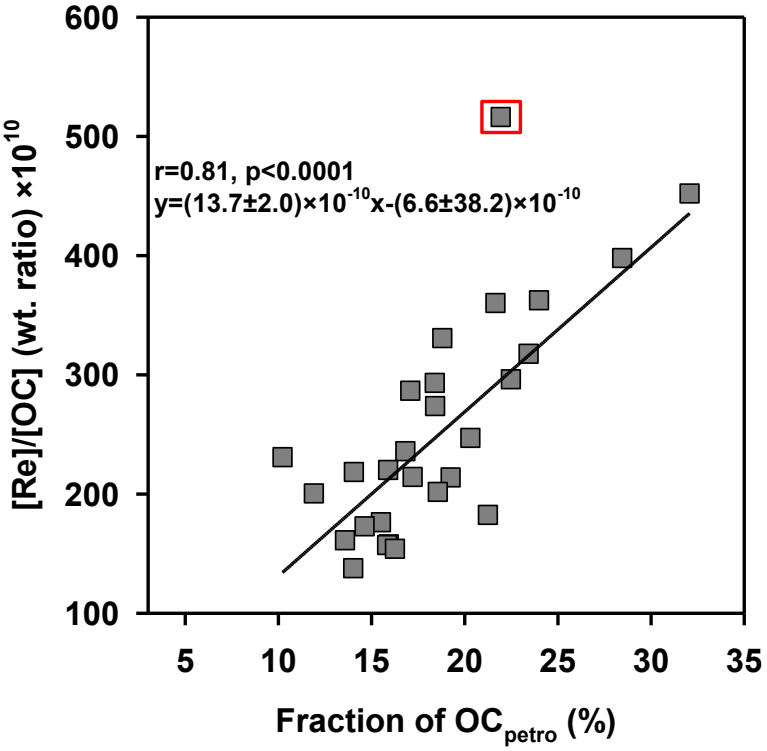

Fig. 7. Variation of [Re]/[OC] ratios with OC_{petro} fractions in the Hooghly River sediments. The data are suggestive of a higher Re/OC ratio for OC_{petro} than for OC_{bio}. The regression of data yields a $[Re/OC]_{petro}$ of $(1.37\pm0.20)\times10^{-7}$ g/g at 100% OC_{petro}. For estimation of OC_{petro} fractions, see supplementary materials (section S10). The line represents the linear regression trend for the combined data from SS and SPM. One outlier (in the box) was excluded from the regression.

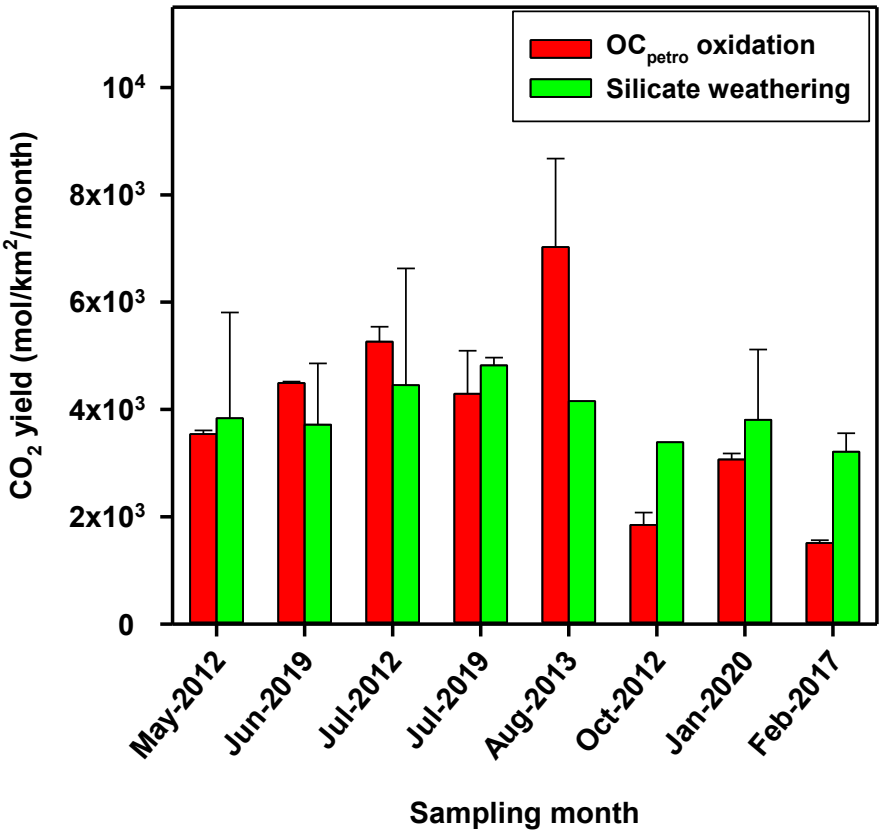

Fig. 8. CO_2 release yield driven by OC_{petro} oxidation and CO_2 drawdown due to silicate weathering in the Ganga–Hooghly River catchment (unpublished data). During high discharge (monsoon) periods, release of CO_2 equals or exceeds its uptake, whereas during low discharge periods, CO_2 consumption dominates over its release. Details of the CO_2 consumption rate calculation are provided in Supplementary materials (section S11).

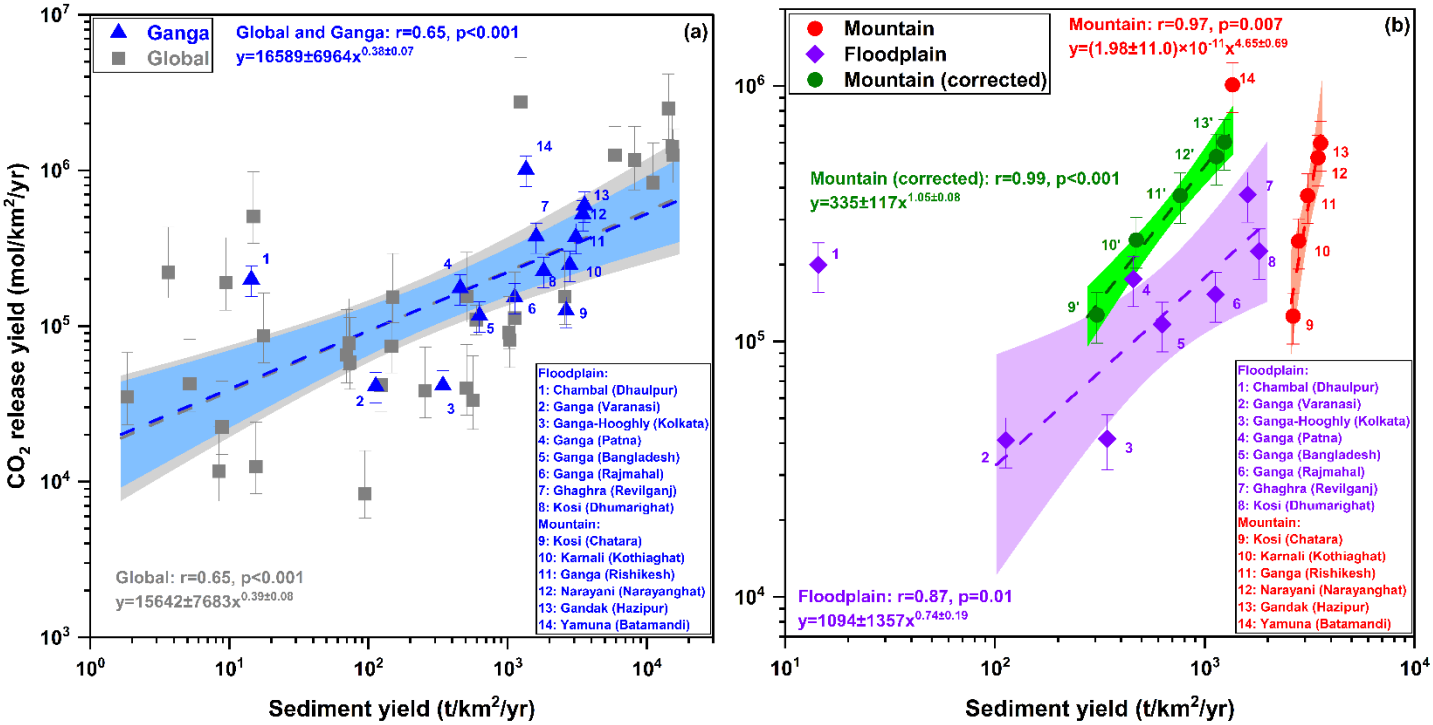

Fig. 9. The CO_2 release yield due to OC_{petro} oxidation vs sediment yield for **(a)** the GHR basin (blue) and global river catchments (grey) and **(b)** floodplain (purple) and mountainous (red) catchments of the GHR basin. The dashed lines represent the power-law regression in each plot. Note that the regression lines for the global (grey) and GHR basin (blue) data overlap. The Yamuna and Chambal basin data are outliers and excluded from regression in (b). For mountainous catchments, the red circles represent the total sediment yields, whereas the green circles are plotted after effecting a correction for non-oxidation of OC_{petro} by subtracting a value of 2324 t/km^2/yr from total sediment yield (see section 5.5 and Supplementary materials Fig. SF8). The shaded regions represent 95% confidence band for regression analysis. The CO_2 release yield (unpublished data) and sediment yield data for different locations in the GHR basin were sourced from Abbas and Subramanian (1984); Lupker et al. (2012a); and Sinha et al. (2005), respectively. Global river catchment data are sourced from Zondervan et al. (2023). For CO_2 release calculations, please see eq. (2) and section 5.4.

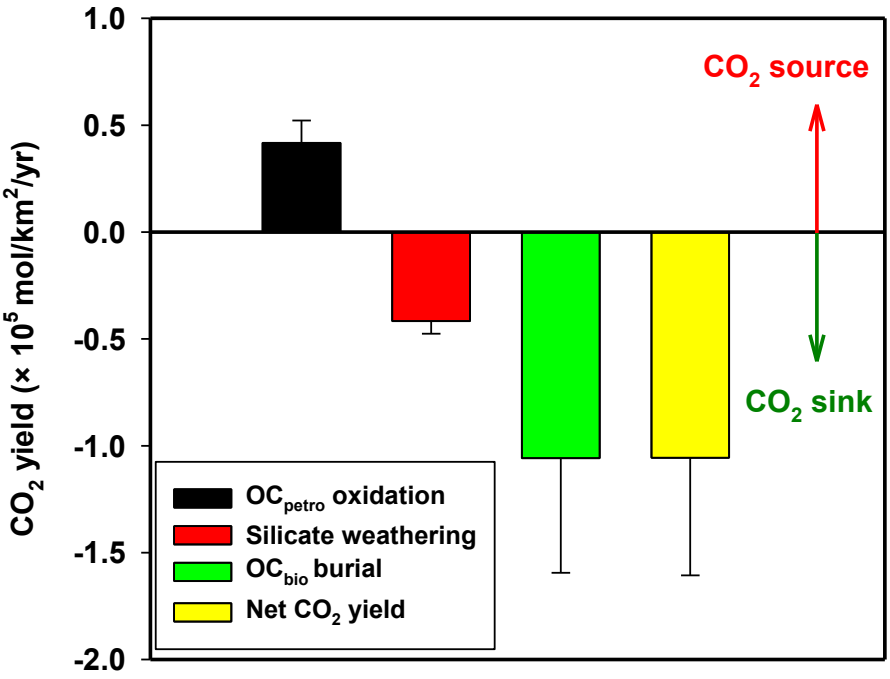

Fig. 10. Net CO_2 balance in the Ganga–Hooghly River catchment. The negative and positive values indicate atmospheric CO_2 consumption (sink) and release (source), respectively. The Ganga–Hooghly River catchment acts as a net sink for CO_2 driven by substantial transport and burial of OC_{bio}.

Supplementary materials for

Petrogenic Carbon Oxidation and Its Impact on the Carbon Balance in the Ganga River Basin

Rupak Samadder[1*], Tarun K. Dalai[1], Kruttika Mohapatra[2], Pankaj Kumar[3], Damodararao Karri[4], Sanjeev Kumar[5]

[1]Department of Earth Sciences, Indian Institute of Science Education and Research Kolkata, Mohanpur 741246, India

[2]Department of Earth and Climate Science, Indian Institute of Science Education and Research Pune, Pune 411008, India

[3]Inter-University Accelerator Centre, New Delhi 110067, India

[4]Center for Climate Change Research, Indian Institute of Tropical Meteorology, Pune 411 008, India

[5]Geosciences Division, Physical Research Laboratory, Navrangpura, Ahmedabad 380009, India

*Corresponding author: Rupak Samadder (rupaksamadder@gmail.com)

Supplementary material includes the following:

Section S12: The CO_2 release due to OC_{petro} oxidation as a function of erosion yield in the mountainous catchments of the Ganga–Hooghly River basin

Section S13: Supplementary Tables (Table ST1-ST2)

Supplementary Materials

S1. Sample collection and processing

Between the years 2012 and 2020, the water and sediment samples in the freshwaters (salinity≤0.3‰) were collected from the Hooghly River between Kolkata and Nischindipur (~90 km downstream of Kolkata, see main text Fig. 1b) covering periods of contrasting discharges, pre-monsoon (PrM: January to June), monsoon (M: July-September), and post-monsoon (PoM: October-December). The sediment samples include both suspended and surface sediments. In addition, groundwater samples from adjacent areas of the Hooghly River and domestic and industrial effluent water samples from Kolkata metropolitan area were collected in the year 2013. The sample collection and processing details for the years 2012 and 2013 are reported in Samanta et al. (2015) and Samanta and Dalai (2016, 2018). A brief account of sampling and sample processing are given below.

Surface water samples were collected in plastic carboys using a boat or jetty to avoid local contamination from the bank. Before collection, carboys were rinsed with the river water at every sampling station. Water samples were filtered through a 0.45 or 0.22 μm Whatman Nucleopore polycarbonate filter in a clean air environment, acidified to <2 pH with Tamapure (AA-100) HNO_3 and stored in precleaned HDPE bottles for major cations and trace elements analysis. The suspended particulate matter (SPM) were collected from water samples after keeping the water samples in plastic carboys to settle overnight, decanting the water, centrifuging the slurry, and washing the sediments with Milli-Q water. During low tide periods, the surface sediments covering

a depth of ~5 cm were collected from the exposed part of river beds using an acrylic scoop. The sediment samples were dried in a hot air oven at 70˚C and powdered to <100 mesh size using an agate pestle mortar assembly or agate planetary disc mill (Retsch RS200) before storing them in plastic containers.

About 60 to 200 mg of sediment powders were dried and treated with 0.5 mL of Suprapur H_2O_2 (Merck) for one hour to oxidize the organic matter. The residues were digested with a mixture of double distilled (DD) HNO_3, HCl, and HF acids in 1:3:1 proportion by volume. The sample digests were dried and redissolved in approximately 30 mL of 5% DD HNO_3 and stored in precleaned HDPE bottle for analysis. Each batch of dissolution included procedural blanks, sample replicates, and certified reference standards.

The concentrations of Re in water and sediment samples were determined by isotope dilution. Accurately weighed ~40-70 g of water samples or digests of 0.1-0.2 g of dry sediment samples were transferred into pre-cleaned Savillex beakers or vials. Each aliquot was spiked with a known quantity of ^{185}Re tracer solution. The spiked sample aliquots were left overnight to equilibrate before being evaporated at 80°C. The dried aliquots were then dissolved in 0.5 mL of 0.5N DD HNO_3 and Re was purified on ion-exchange columns following methods modified after Dalai et al. (2002), Miller et al. (2011), and Rahaman and Singh (2010). The procedural blanks were prepared for each batch of samples, and some samples were processed in replicates. Purified Re aliquots were dried at 70˚C, redissolved in 5% DD HNO_3 before measuring their $^{185}Re/^{187}Re$ ratios.

For measurement of radiocarbon content (percentage modern carbon, pMC) in organic matter, the sediment samples were prepared following the protocol modified after Sharma et al. (2019) and Kumar et al. (2022). Powdered samples (1–3 g) were dried in a hot air oven at 70°C

and transferred to centrifuge tubes. In these tubes, the samples were decarbonated by adding 1N DD HCl and placing them on a shaker for ~1 hour at 60°C and 600 rpm. The process was repeated multiple times until no effervescence was observed. The acid-treated samples were then rinsed with Milli-Q water multiple times until the sediment pH reached ~7 and subsequently freeze-dried overnight to remove any remaining water.

The above-described dried pretreated samples were packed in tin capsules and placed in the auto-sampler of the elemental analyzer (EA) of the automated graphitization equipment (AGE). The graphitization process involved combustion at 900°C in the presence of O_2 to produce CO_2, which was purified by passing through columns (please see Němec et al. (2010) for details). The purified CO_2 was transferred to a glass tube filled with pure catalyst iron powder and reacted with H_2 gas at 580°C to form graphite. Water vapors, a byproduct of the aforementioned reduction reaction, were removed with the help of peltier coolers mounted on the top of the reaction tube in AGE. The prepared graphite was then pressed into cathode capsules for radiocarbon measurement using the Accelerator Mass Spectrometry (AMS) facility at the Inter-University Accelerator Centre (IUAC) Delhi.

S2. Analytical methods

Temperature, pH, total dissolved solids (TDS), salinity, conductivity, and dissolved oxygen (DO) were measured in situ using portable multi-electrode probes (Eutech PCSTestr 35 and Hach HQ40d). The concentrations of HCO_3^- and CO_3^{2-} were measured by manual acid-base titration in the field and an auto titrator (Metrohm 916 Ti-touch) in the lab. The major anion and cation concentrations were measured by an ion chromatograph (Themo Scientific Dionex ICS-5000). The accuracy and precision of measurement for anions and cations are better than ±10% and ±7%, respectively. In sediment samples, the concentrations of Al, Na, K, Ca, and Cs were measured

using a quadrupole ICP-MS (X series 2, Thermo Scientific) facility at the Indian Institute of Science Education and Research (IISER) Kolkata. The internal standards Indium (In) or Ruthenium (Ru) was added to the samples, standards, and blanks for correcting instrumental drift during analysis. The reference standards SBC-1 (brush creek shale), GSP-2 (granodiorite), MESS-3 (marine sediment), JSD-3 (stream sediment) and SDC-1 (mica schist) were analyzed to assess analytical accuracy, while replicate analyses of samples were performed to evaluate analytical precision. The accuracy and precision for all the elements are within ±10% and ±7%, respectively. The concentrations of Si in the surface sediments were measured using an X-ray Fluorescence Spectrometer (Bruker Tiger S-8 WD) at IISER Kolkata with accuracy and precision better than 5%.

The OC concentrations and $\delta^{13}C_{org}$ in sediment samples were measured using isotope ratio mass spectrometry (IRMS) facilities at Physical Research Laboratory (PRL), Ahmedabad and IISER Pune. Prior to the analysis, samples were decarbonated using 1N DD HCl to remove inorganic carbon. The decarbonated sediments were combusted at 1150˚ C, and the released CO_2 were analyzed for [OC] and $\delta^{13}C_{org}$ (reported relative to Vienna Pee Dee Belemnite,VPDB) using an elemental analyzer coupled to an IRMS. Cellulose standard IAEA-CH-3 ($\delta^{13}C$ = −24.72‰; C content = ~44.4 wt.%) and USGS shale standard SGR-1b ($\delta^{13}C$ = -25.02±0.47‰; C content = 27.40±0.46 wt.%; Stüeken et al. (2020)) were analyzed to assess analytical accuracy. Based on the measurements of these standards, the accuracy is better than 3% for total carbon and 0.2‰ for $\delta^{13}C$. Replicate analyses of the samples indicate a precision better than 5% for [OC] and 0.8‰ for $\delta^{13}C_{org}$.

The Re concentrations of water and sediment samples were determined by measuring $^{185}Re/^{187}Re$ ratios by a quadrupole ICP-MS facility at IISER Kolkata. The background signals

(CPS) for ^{185}Re and ^{187}Re were in single digits, while sample signals (CPS) were in the 10^4-10^6 range. The procedural blank for analysis of dissolved Re was 0.46±0.31 pg (1 SD, n=4), which is less than 0.7% of the lowest Re mass analyzed. Therefore, the measured dissolved [Re] values were not corrected for blank contributions. The precision of measurement based on the replicate analysis is within ±5% (n=3). A spiked solution of the Re standard NIST 3143 was analyzed after every 8-10 samples. The Re concentration of this standard was measured with an accuracy of ±2% (n=24).

For sediment samples, the background Re signals were in single digits, and Re signals for samples were higher by four to six orders of magnitudes. The procedural blanks ranged from 0.25-1.51 pg (n=2), which accounts for less than 2% of the Re mass in the processed samples aliquots. Based on the replicate analysis of sediment samples, the precision of Re measurement is better than 8% (n=4). The measured Re concentration in the reference standard SBC-1 is 11.1±0.4 ng/g (1 SD, n=6), which is in excellent agreement with the published value of 11.1±0.2 ng/g (Li and Yin, 2019).

Radiocarbon measurements were conducted on the prepared graphite samples (section S1) by using a 500 kV Pelletron accelerator. The AMS was calibrated with alpha graphite, OXII standards, and phthalic anhydride (Ph) blanks. The measured $^{14}C/^{12}C$ ratios for samples, standards, and blanks were normalized to the OXII standard value. The $\delta^{13}C$ values were normalized to -25‰ to account for isotopic fractionation during sample processing and measurements. The analytical background was 0.602±0.0156 pMC, corresponding to a $^{14}C/^{12}C$ ratio of $(5.6132\pm0.1444)\times10^{-15}$. A secondary standard, IAEA C7, was also analyzed for additional check on data quality, yielding a pMC value of 49.12±0.35, which closely matched the consensus value of 49.53±0.12. The ^{14}C activity in the replicates of a sample agreed within 0.15%.

S3. Concentrations of Re in the Hooghly River water and sediment samples

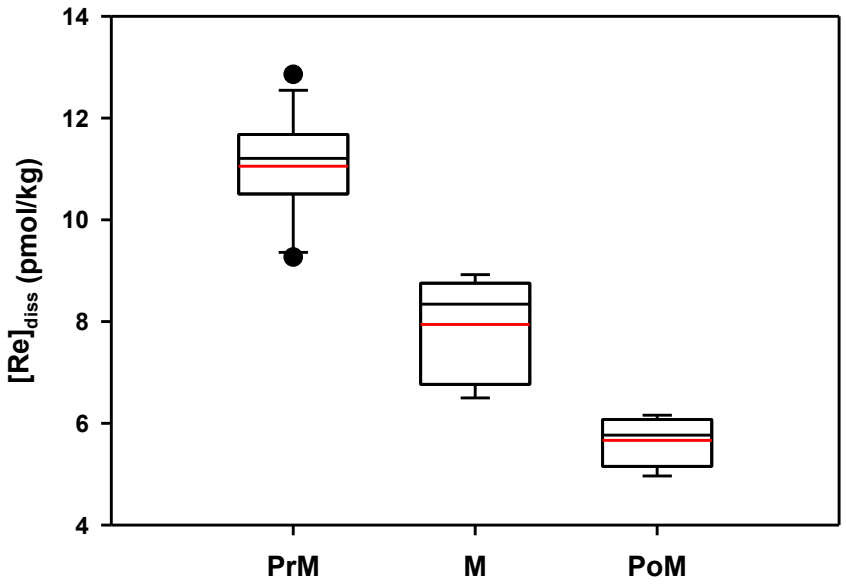

Fig. SF1. Box and whisker plots showing seasonal variation of $[Re]_{diss}$ in the Hooghly River. The plots illustrate the interquartile ranges (box), the 10th and 90th percentiles (whiskers), the mean (red lines), the median (black line), and outliers (black circles). PrM: pre-monsoon, M: Monsoon, PoM: post-monsoon.

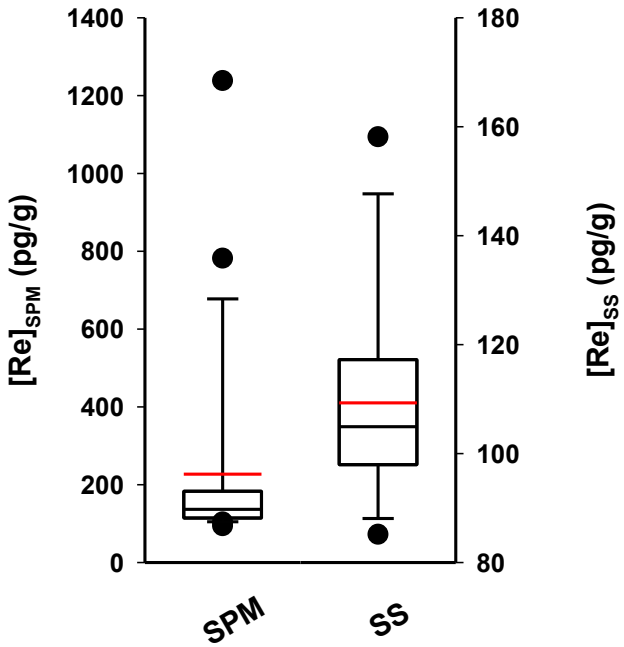

Fig. SF2. Box and whisker plots showing [Re] in the Hooghly River sediments (SPM: suspended particulate matter, SS: surface sediments). The plots illustrate the interquartile ranges (box), the

10th and 90th percentiles (whiskers), the mean (red line), the median (black line), and outliers (black circles).

S4. Variation of [Re]/[Al] with [Cs]/[Al] in the Hooghly River sediments

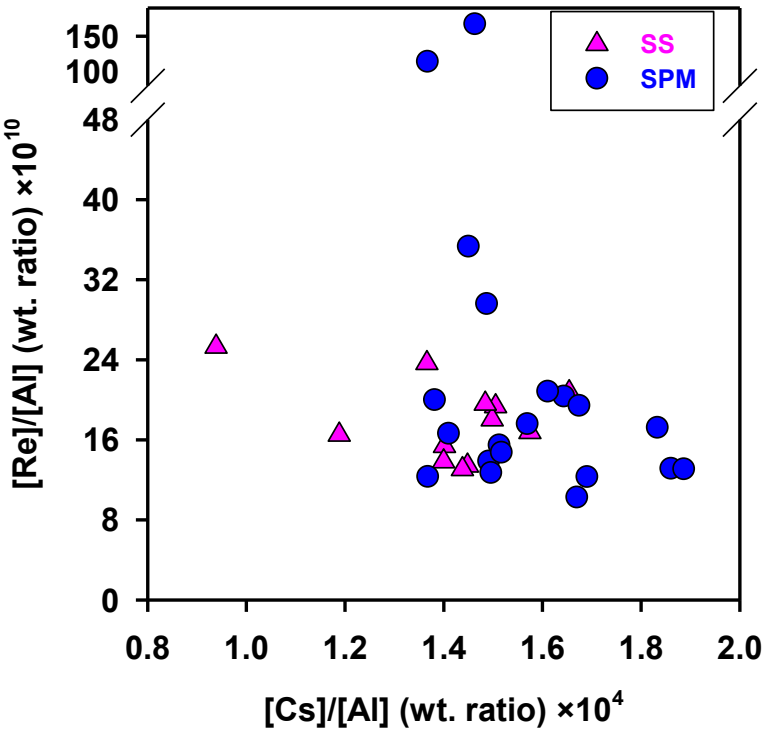

Fig. SF3. Variation of [Re]/[Al] with [Cs]/[Al] in the Hooghly River sediments (SS: surface sediments, SPM: suspended particulate matter). The absence of any significant positive correlation suggests that sedimentary Re is insignificantly influenced by solute-particle interaction processes such as adsorption.

S5. Variation of [Mg]/[Na] vs. [Ca]/[Na] ratios in the Hooghly River water

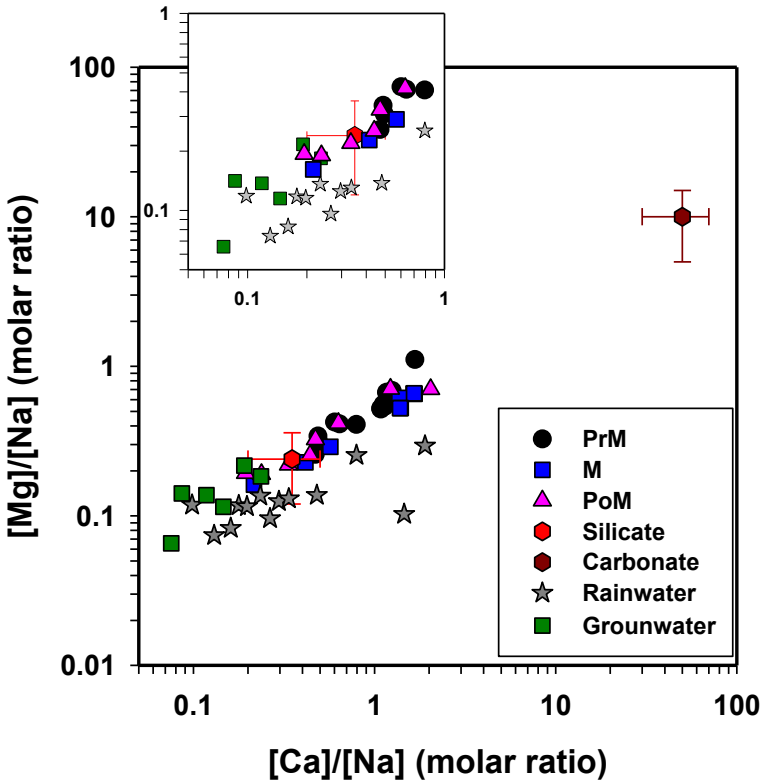

Fig. SF4. Variation of [Mg]/[Na] vs. [Ca]/[Na] ratios in the Hooghly River water and groundwater samples (green squares). The rainwater (stars) composition data are sourced from Majumdar et al. (2020), and silicate and carbonate compositions (hexagons) from Gaillardet et al. (1999). The inset shows the distribution of data points at lower [Mg]/[Na] and [Ca]/[Na] values for clarity.

S6. Variation of [OC]/[Al] ratios with CIA in the Hooghly River sediments

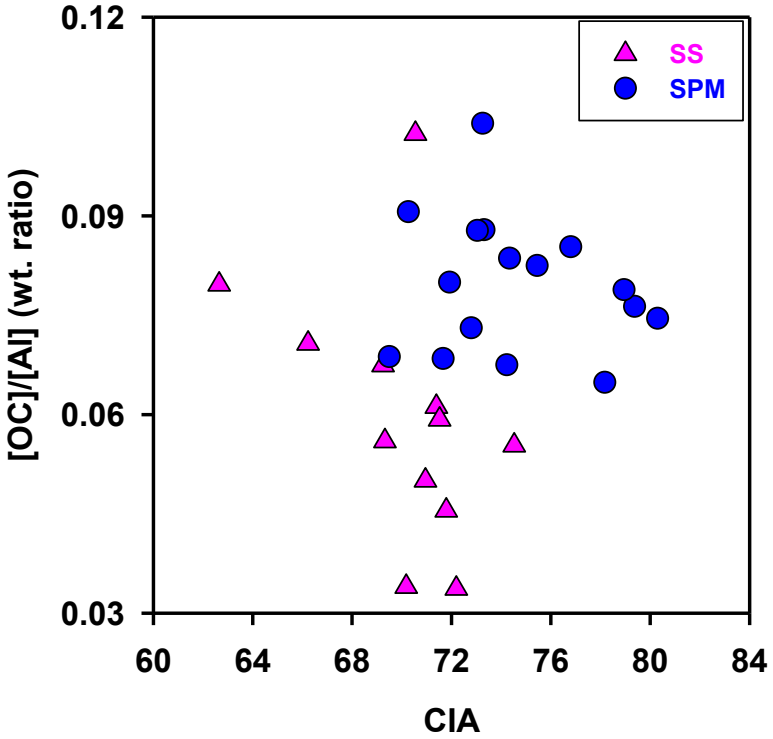

Fig. SF5. Variation of [OC]/[Al] ratios with CIA in the Hooghly River sediments (SPM: suspended particulate matter, SS: surface sediment). The scattered distribution is inferred to result from differences in the OC sources: OC_{petro} is associated with major lithologies, whereas OC_{bio} is not. Samples in the shaded region show ~3-fold variation in OC/Al ratio over a narrow CIA range (see main text section 5.2.4).

S7. Fraction of dissolved Re contribution from non-cyclic sources

In this section, we quantify contributions from various sources to the dissolved Re budget. The potential sources of dissolved Re are silicates, carbonates, sulfides, $OC_{petro,}$ and anthropogenic inputs (Dalai et al., 2002; Dellinger et al., 2023; Horan et al., 2019; Miller et al., 2011; Rahaman et al., 2012). Additionally, dissolution of evaporites, rainwater, and saline groundwater can influence solute concentrations including that of Re. Therefore, we determine the solute contributions from non-cyclic sources by using [Cl] as an index.

$$[X]_{non\text{-}cyclic} = [X]_{river} - \left(\left[\frac{X}{Cl}\right]_{cyclic} \times [Cl]_{river}\right) \quad (s1)$$

where [X] denotes the concentration of a solute. We assume that $[Cl]_{river}$ is derived exclusively from cyclic sources (rains, evaporites, and saline groundwater). The Re/Cl ratios of Hooghly River water are indicative of mixing of saline groundwater with low Re/Cl with inputs from non-cyclic sources having high Re/Cl ratios (see main text section 5.2.3). The Re/Cl ratios (pmol/μmol) of these saline groundwater samples are in the range of $(0.4\text{-}45)\times10^{-5}$, which are more than ~4 times lower than those in the Hooghly River waters. The elevated Re/Cl ratios in the river water indicate that Re contribution from cyclic sources is insignificant. Based on Re/Cl ratios of groundwater samples, the estimated Re contributions from the cycling sources, are in range of 1-14%. For cyclic correction of Na and SO_4, we use the molar ratios of Na/Cl=1 (maximum Na/Cl ratio in evaporites) and SO_4/Cl=0.05 (seawater) for the cyclic end member composition. These values were utilized considering the proximity of the study area to the Bay of Bengal. Using these molar ratios of Na/Cl and SO_4/Cl in eq. (s1), it is estimated that cyclic sources account for at least 50% of Na and at best 60% of SO_4 in the Hooghly River waters.

Among the non-cyclic sources of Re (silicates, carbonates, sulfides, anthropogenic and OC_{petro}), carbonate rocks are a minor contributor to the dissolved Re pool as evident from their mean Re/Ca molar ratio of 5.6×10^{-5} pmol/μmol in the Lesser Himalayan carbonates, which are about an order of magnitude lower than that in silicate rocks in the Himalayas (5.8×10^{-4} pmol/μmol, Dalai et al. (2002)). Using the mean Re/Ca ratio in the carbonates and assuming that all dissolved Ca is derived from carbonate weathering, the estimated carbonate contribution accounts for <1% of dissolved Re in the Hooghly River. However, if dissolved Ca is partitioned into the exchangeable phases (Lupker et al., 2016; Tipper et al., 2021), the carbonate contribution

can be higher, upto ~1% of the dissolved [Re] in the river water. Nevertheless, given that Ca can also be supplied by silicate rocks, the above estimate can be considered as the *upper limit* of Re contributions from carbonate weathering. Based on the approach of Horan et al. (2019), we determine below Re contributions from silicates, sulfides, and OC_{petro} weathering by assuming that Re, Na, and S are released during weathering in the same proportion as in the source rocks. As dissolved Re, Na, and SO_4 behave nearly conservatively in oxygenated aqueous environments (Anbar et al., 1992; Burt et al., 2021; Colodner et al., 1993; Gaillardet et al., 1999; Hodge et al., 1996; Kaste et al., 2016; Rahaman and Singh, 2010), $[Re]_{diss}$ contributions from silicate and sulfide sources can be quantified based on the following relations (eq. s2-3), with the assumption that non-cyclic Na and SO_4 are supplied by silicate and sulfide weathering, respectively.

$$[Re]_{silicates} = \left(\frac{Re}{Na}\right)_{silicates} \times [Na]_{non\text{-}cyclic} \quad (s2)$$

$$[Re]_{sulfides} = \left(\frac{Re}{S}\right)_{sulfides} \times [SO_4^{2-}]_{non\text{-}cyclic} \quad (s3)$$

where subscripts 'non-cyclic', 'silicates', and 'sulfides' represent non-cyclic, silicate, and sulfide minerals sources, respectively. The concentrations and ratios in the above equations are all molar. The non-cyclic Re in river waters, which is the cumulative contributions from silicate, sulfide, $OC_{petro,}$ and anthropogenic sources, can be expressed as:

$$[Re]_{non\text{-}cyclic} = [Re]_{silicates} + [Re]_{sulfides} + [Re]_{petro} + [Re]_{anth} \quad (s4)$$

The Re/Na ratios in the silicates are in the range of 0.5×10^{-4} to 2×10^{-4} pmol/μmol, as reported for the Himalayan granites (Dalai et al., 2002). These values are two orders of magnitude lower than the dissolved Re/Na* ratios in the Hooghly River. The sulfide minerals typically exhibit lower Re/S ratio compared to OC_{petro} and silicates (Horan et al., 2019). In the Amazon River basin, based

on the data on tributaries draining sulfide-rich lithologies, Dellinger et al. (2023) inferred that the Re/S ratios in sulfide minerals are in the range of 0.2×10^{-3} to 4×10^{-3} pmol/μmol. The Re/SO_4^{2-} ratios (0.03-0.07 pmol/μmol) in the Hooghly River waters are more than an order of magnitude higher than the maximum sulfide Re/S ratio reported by Dellinger et al. (2023) and 15-35 times higher than the sulfide Re/S ratio (0.001-0.002 pmol/μmol) reported by Horan et al. (2019) and Rout and Tripathy (2024). Using the molar ratios (pmol/μmol) of Re/Na in the range of $(0.5\text{-}2.0)\times10^{-4}$ for silicates and Re/S ratios in the range of $(0.2\text{-}4.0)\times10^{-3}$ for sulfide minerals in eq. (s3-4), we calculate the fractional Re contributions as follows:

$$f_x = \left(\frac{[Re]_x}{[Re]_{diss}}\right) \qquad (s5)$$

where f is the mass fraction, subscript 'x' denotes a source (silicates, sulfides, anthropogenic, and OC_{petro}) of dissolved Re. All calculations (eq. s1-5) were performed using a Monte Carlo simulation, with ten thousand iterations for data of each sample. This simulation uses a random distribution of Re/S ratios in sulfide and Re/Na ratios in silicate end-members (Dellinger et al., 2023). Therefore, variability and uncertainty in Re contributions from different sources are accounted for, providing a more robust estimate of dissolved Re contribution from each source.

Our calculations (eq. s5) show that weathering of silicates, sulfides, and OC_{petro} contributes to <1%, 2-6%, and 74-92%, respectively to the dissolved Re budget of the Hooghly River (unpublished data). Following the same approach and using reported Re and major ion concentrations of the Ganga River and their tributaries (Dalai et al., 2002; Miller et al., 2011; Rahaman et al., 2012), we estimate that OC_{petro} oxidation contributes up to 97% of the dissolved Re in these rivers (unpublished data). These calculations assume that Re contributions from anthropogenic sources in the upper reaches of the Yamuna and Ganga Rivers are negligible.

S8. Estimation of monthly water discharge of the Hooghly River for the years 2013-2020

The Hooghly River water discharge at Gangasagar (Rudra, 2014) shows a strong positive correlation with rainfall for the year 2012 (Fig. SF6). Such an observation underscores the role of rainfall in regulating water discharge within the Hooghly River catchment and is also consistent with studies highlighting rainfall as the dominant driver of water discharge in the Himalayan and Indian River systems (Bookhagen and Burbank, 2010; Jana et al., 2021; Varikoden and Revadekar, 2020). We calculated monthly water discharge at Ganganagar using regression parameters from Fig. SF6 and monthly rainfall data for the catchment for the years 2013-2020 (IMD, 2014, 2016a, b, 2017, 2018, 2020, 2021a, b). The monthly river water discharge at Nabadwip, were calculated using the estimated rainfall at Gangasagar and ratio of discharge values at Nabadwip and Gangasagar for the year 2012 reported by Rudra (2014). The estimated annual water discharge of the Hooghly River at Nabadwip varies from (68.8-93.1)$\times 10^9$ m^3/year for the years 2012-2020, with an average of (78.6±7.9)$\times 10^9$ m^3/year.

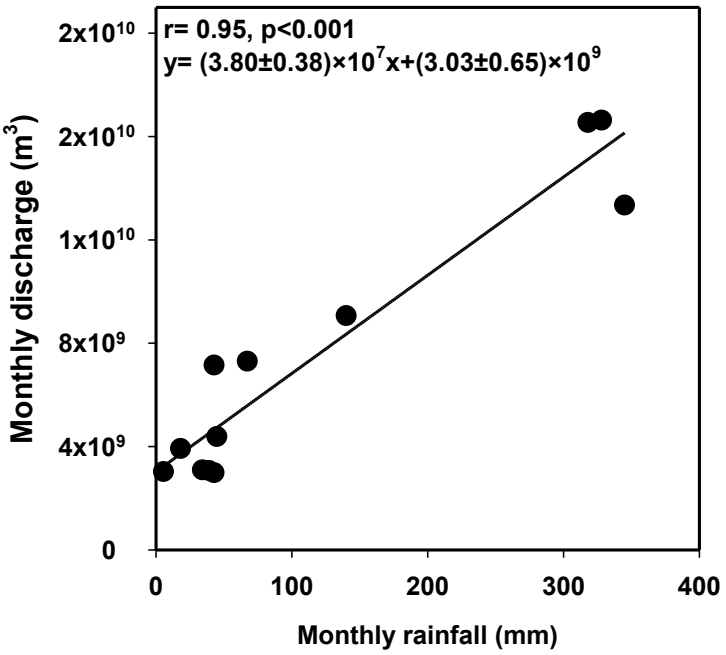

Fig. SF6. Variation of monthly water discharge of the Hooghly River at Gangasagar in 2012 (Rudra, 2014) with monthly rainfall data of the year 2012 (IMD, 2013).

S9. Estimation of dissolved Re flux

Dissolved Re flux was determined using $[Re]_{diss}$ of each period (this study) and the monthly water discharge (section S8). The estimated dissolved Re fluxes, based on data of eight different months during the period (2012-2020) exhibit seasonal variation, with a peak value of ~120 mol/month during the monsoon period (August 2013) and the lowest value of ~25 mol/month during the pre-monsoon period (February 2017). Using the monthly water discharge (section S8) and average $[Re]_{diss}$ of each sampling period, we calculated the discharge weighted $[Re]_{diss}$ of Hooghly River to be 8.6±0.2 pmol/kg. Based on this $[Re]_{diss}$ value and average annual water discharge at Nabadwip for years 2012-2020 (section S8), the dissolved Re flux is estimated to be 675±70 mol/yr, and the dissolved Re yield is $(7.0\pm0.7)\times10^{-4}$ mol/km^2/yr for the Ganga–Hooghly River (GHR) catchment.

S10. Estimation of $[OC]_{petro}$ in the Hooghly River sediments

The radiocarbon activity of OC and [OC] in the sediments were utilized to determine the amount of OC_{petro}. This approach is based on two key assumptions: (i) the [OC] is a combination of $[OC]_{petro}$ and $[OC]_{bio}$, and (ii) the radiocarbon composition (expressed as percentage modern carbon, pMC) of OC_{petro} is lower than the analytical detection limit (pMC=0). Therefore, mass balance of [OC] and pMC can be expressed as the following (Galy et al., 2008a):

$$[OC] = [OC]_{petro} + [OC]_{bio} \qquad \text{(s6)}$$

$$pMC = pMC_{petro} \times \left(\frac{[OC]_{petro}}{[OC]}\right) + pMC_{bio} \times \left(\frac{[OC]_{bio}}{[OC]}\right) \qquad \text{(s7)}$$

substituting $pMC_{petro} = 0$, we get

$$pMC \times [OC] = \left(pMC_{bio} \times [OC]\right) - \left(pMC_{bio} \times [OC]_{petro}\right) \qquad \text{(s8)}$$

where the subscripts 'bio' and 'petro' represent biospheric and petrogenic organic carbon, respectively. The $[OC]_{petro}$ is determined from the intercept (= $pMC_{bio} \times [OC]_{petro}$) and slope (= pMC_{bio}) in a plot of pMC×[OC] vs [OC] (Fig. SF7). We estimate that $[OC]_{petro}$ in SPM and surface sediments of the Hooghly River is 0.11±0.07 wt.% and 0.07±0.02 wt.%, respectively, which correspond to 12-23% of the total [OC] in SPM and 10-32% in surface sediments. These $[OC]_{petro}$ values are a 2 to 4 times higher than those reported for Ganga River sediments in Bangladesh, with an average $[OC]_{petro}$ of 0.025% (Galy et al., 2008a). However, the fraction of OC_{petro} in the Hooghly River surface sediments partially overlaps with and is comparable to the lower end of the OC_{petro} range (17-83%) reported for surface sediments of the Ganga River in Bangladesh. In contrast, the fractional OC_{petro} abundances in the SPM of the Hooghly River (12-23%) are higher than those in the SPM of the Ganga River (4-11%) in Bangladesh (Galy et al., 2008a).

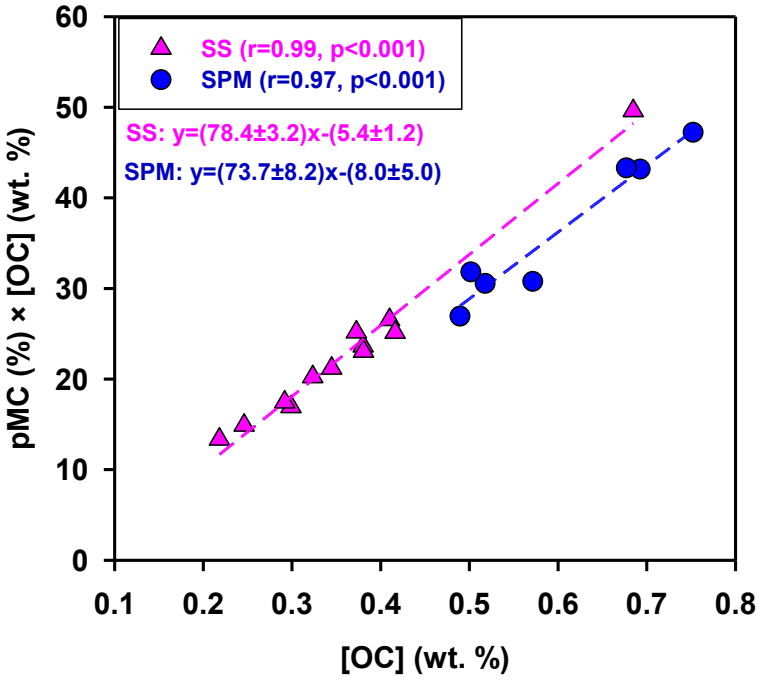

Fig. SF7. Plot of pMC × [OC] vs [OC] of the Hooghly River sediments (SPM: suspended particulate matter, SS: surface sediment).

S11. Estimation of CO_2 consumption due to silicate weathering in the Ganga–Hooghly River catchment

Major cations Na, K, Ca, and Mg concentrations of river water are widely used to estimate silicate weathering rates (Tripathy and Singh, 2010) because they can be predominantly derived from chemical weathering of silicate rocks. However, these cations can be derived from other sources such as (i) dissolution of carbonate rocks, which primarily supplies Ca and Mg (ii) dissolution of evaporites and (iii) cyclic inputs. In order to quantify the silicate-derived component for each of these cations, we use a forward model following the approach of Krishnaswami and Singh (1998), and Galy and France-Lanord (1999). This model assumes Na is derived from silicate, evaporite and cyclic sources. To distinguish silicate-derived Na from other sources, we use Cl as an index for cyclic sources. The Na contribution from silicate sources is expressed as:

$$[Na]_{sil} = [Na]_{river} - \left(\left[\frac{Na}{Cl}\right]_{cylic/ev} \times [Cl]_{river}\right) \qquad (s9)$$

where, [] denotes concentration of solute, subscript 'sil', 'river', 'cyclic' and 'ev' represents silicate, river water, cyclic source, and evaporite sources, respectively. For the cyclic source, we use the molar ratio of Na/Cl =1. To determine K contribution from silicate sources, we assume that it is exclusively supplied to the river via silicate weathering.

$$[K]_{sil} = [K]_{river} \qquad (s10)$$

The Ca and Mg contribution from silicate (Ca_{sil} and Mg_{sil}) can be estimated using $[Na]_{sil}$, $[Ca/Na]_{sol}$ and $[Mg/Na]_{sol}$ following approach of Krishnaswami and Singh (1998):

$$[Ca]_{sil} = \left[\frac{Ca}{Na}\right]_{sol} \times [Na]_{sil} \qquad (s11)$$

$$[Mg]_{sil} = \left[\frac{Mg}{Na}\right]_{sol} \times [Na]_{sil} \qquad (s12)$$

where $[Ca/Na]_{sol}$ and $[Mg/Na]_{sol}$ are the molar ratios released to river waters from silicate weathering. For this study, we used a value of 0.7±0.3 for $[Ca/Na]_{sol}$ and 0.3±0.2 for $[Mg/Na]_{sol}$, which are determined based on evaluation of composition of bed-rock (granites/gneisses and metasediments of the Higher and Lesser Himalya), soil profiles and rivers draining predominantly the silicate lithology (Krishnaswami and Singh, 1998).

The silicate weathering rate (SWR, t/km^2/yr) and CO_2 consumption rate during silicate weathering (mol/km^2/yr) in a river catchment can be expressed as (Tripathy and Singh, 2010)

$$SWR = \frac{Q}{A} \times ([Na]_{sil} + [K]_{sil} + [Ca]_{sil} + [Mg]_{sil}) \qquad (s13)$$

$$CO_2 \text{consumption rate} = \frac{Q}{A} \times \left([Na]_{sil} + [K]_{sil} + 2 \times ([Ca]_{sil} + [Mg]_{sil})\right) \qquad (s14)$$

where Q (L/yr) and A (km^2) represent river water discharge and catchment area, respectively. The units of concentrations are mg/L in eq. (s13) and μEq/L in eq. (s14). The river water discharge estimated in section S8 were used for calculations of CO_2 consumption rate due to silicate weathering in the Ganga–Hooghly River catchment.

S12. The CO_2 release due to OC_{petro} oxidation as a function of erosion yield in the mountainous catchments of the Ganga–Hooghly River basin

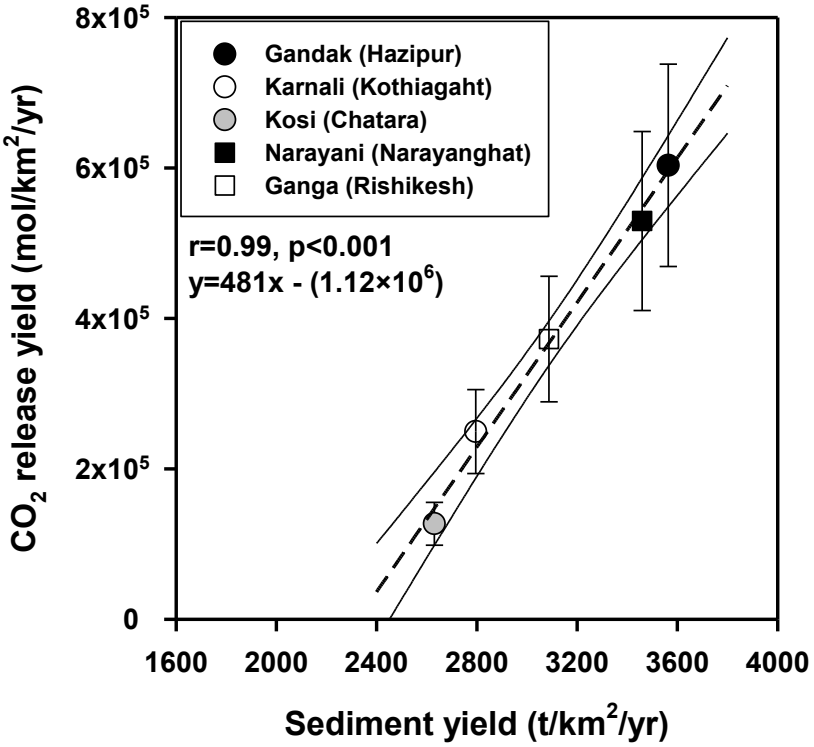

Fig. SF8. The yield of CO_2 release due to OC_{petro} oxidation vs sediment yield in the mountainous catchments (>2000 t/km^2/yr) of the Ganga River basin. The linear regression and the 95% confidence bands are marked by dashed and solid lines, respectively. The x-intercept value (2324 t/km^2/yr) provides a measure of the catchment-average sediment yield associated with no OC_{petro} oxidation (see section 5.5 in the main text).

S13. Supplementary Tables

Table ST1. Comparison of Re/ΣCations* ratios of river water with Re/ΣCations ratios reported of silicate and carbonate rocks. The Re/ΣCations of carbonate and silicate rock sourced from Dalai et al. (2002).

	Range	Mean±SD
	(Re/ΣCations)×10^{-10} (molar ratio)	
Hooghly River waters[a]	44-254	79±42
Silicates	0.3-1.0	0.5±0.4
Carbonates	0-1.1	0.3±0.4

[a][Na] in ΣCations corrected for cyclic contribution.

Table ST2. Comparison of $[Re/OC]_{petro}$ ratio in the Ganga–Hooghly River catchment with Lesser Himalayan black shales and world river basins.

River basins/Black shales	Range or mean of $[Re/OC]_{petro}$ (×10^{-7} g/g)	References
Ganga-Hooghly River basin	1.37±.20	this study
Lesser Himalayan black shales	0.7-66	Pierson-Wickmann et al. (2002) and Singh et al. (1999)
Taiwanese River basins	2.6-4.6	Hilton et al. (2014)
Mackenzie River basin	4.8±0.9	Horan et al. (2019)
Swiss Alps	1.8-8.4	Hilton et al. (2021)
Amazon River basin	0.27-7.52	Dellinger et al. (2023)
Tibetan Plateau	0.30-7.52	Wang et al. (2025)

References

Abbas, N., Subramanian, V., 1984. Erosion and sediment transport in the Ganges river basin (India). Journal of Hydrology 69(1), 173-182. https://doi.org/10.1016/0022-1694(84)90162-8.

Allison, M.A., Khan, S.R., Goodbred, S.L., Kuehl, S.A., 2003. Stratigraphic evolution of the late Holocene Ganges–Brahmaputra lower delta plain. Sedimentary Geology 155(3), 317-342. https://doi.org/10.1016/S0037-0738(02)00185-9.

Anbar, A.D., Creaser, R.A., Papanastassiou, D.A., Wasserburg, G.J., 1992. Rhenium in seawater: Confirmation of generally conservative behavior. Geochimica et Cosmochimica Acta 56(11), 4099-4103. https://doi.org/10.1016/0016-7037(92)90021-A.

Baioumy, H.M., Eglinton, L.B., Peucker-Ehrenbrink, B., 2011. Rhenium–osmium isotope and platinum group element systematics of marine vs. non-marine organic-rich sediments and coals from Egypt. Chemical Geology 285(1), 70-81. https://doi.org/10.1016/j.chemgeo.2011.02.026.

Barton, I.F., Rathkopf, C.A., Barton, M.D., 2020. Rhenium in Molybdenite: a Database Approach to Identifying Geochemical Controls on the Distribution of a Critical Element. Mining, Metallurgy & Exploration 37(1), 21-37. https://doi.org/10.1007/s42461-019-00145-0.

Bolton, E.W., Berner, R.A., Petsch, S.T., 2006. The Weathering of Sedimentary Organic Matter as a Control on Atmospheric O2: II. Theoretical Modeling. American Journal of Science 306(8), 575-615. https://doi.org/10.2475/08.2006.01.

Bookhagen, B., Burbank, D.W., 2010. Toward a complete Himalayan hydrological budget: Spatiotemporal distribution of snowmelt and rainfall and their impact on river discharge. Journal of Geophysical Research: Earth Surface 115(F3). https://doi.org/10.1029/2009JF001426.

Bouchez, J., Beyssac, O., Galy, V., Gaillardet, J., France-Lanord, C., Maurice, L., Moreira-Turcq, P., 2010. Oxidation of petrogenic organic carbon in the Amazon floodplain as a source of atmospheric CO2. Geology 38(3), 255-258. 10.1130/G30608.1.

Brookins, D.G., 1986. Rhenium as analog for fissiogenic technetium: Eh-pH diagram (25°C, 1 bar) constraints. Applied Geochemistry 1(4), 513-517. https://doi.org/10.1016/0883-2927(86)90056-9.

Burt, E.I., Bill, M., Conrad, M.E., Quispe, A.J.C., Christensen, J.N., Hilton, R.G., Dellinger, M., West, A.J., 2021. Conservative transport of dissolved sulfate across the Rio Madre de Dios floodplain in Peru. Geology 49(9), 1064-1068. https://doi.org/10.1130/G48997.1.

Central Pollution Control Board, B., 2020. Status of post-monsoon 2020 monitored drains discharging into River Ganga and its tributaries. Central Pollution Control Board, New Delhi, India.

Chakrapani, G.J., Gaillardet, J., Dupre, B., Allegre, C.J., 2002. Osmium isotopic compositions in Ganga river sediments. Current Science 83(10), 1253-1255. https://www.jstor.org/stable/24106480.

Chang, S., Berner, R.A., 1999. Coal weathering and the geochemical carbon cycle. Geochimica et Cosmochimica Acta 63(19), 3301-3310. https://doi.org/10.1016/S0016-7037(99)00252-5.

Chappaz, A., Gobeil, C., Tessier, A., 2008. Sequestration mechanisms and anthropogenic inputs of rhenium in sediments from Eastern Canada lakes. Geochimica et Cosmochimica Acta 72(24), 6027-6036. https://doi.org/10.1016/j.gca.2008.10.003.

Chen, X., Lin, J., Wang, P., Zhang, S., Liu, D., Zhu, B., 2022. Resistant soil carbon is more vulnerable to priming effect than active soil carbon. Soil Biology and Biochemistry 168, 108619. https://doi.org/10.1016/j.soilbio.2022.108619.

Colodner, D., Edmond, J., Boyle, E., 1995. Rhenium in the Black Sea: comparison with molybdenum and uranium. Earth and Planetary Science Letters 131(1), 1-15. https://doi.org/10.1016/0012-821X(95)00010-A.
Colodner, D., Sachs, J., Ravizza, G., Turekian, K., Edmond, J., Boyle, E., 1993. The geochemical cycle of rhenium: a reconnaissance. Earth and Planetary Science Letters 117(1), 205-221. https://doi.org/10.1016/0012-821X(93)90127-U.
Crusius, J., Calvert, S., Pedersen, T., Sage, D., 1996. Rhenium and molybdenum enrichments in sediments as indicators of oxic, suboxic and sulfidic conditions of deposition. Earth and Planetary Science Letters 145(1), 65-78. https://doi.org/10.1016/S0012-821X(96)00204-X.
Dalai, T.K., Singh, S.K., Trivedi, J.R., Krishnaswami, S., 2002. Dissolved rhenium in the Yamuna river system and the Ganga in the Himalaya: role of black shale weathering on the budgets of Re, Os, and U in rivers and CO2 in the atmosphere. Geochimica et Cosmochimica Acta 66(1), 29-43. https://doi.org/10.1016/S0016-7037(01)00747-5.
Danish, M., Tripathy, G.R., Mitra, S., Rout, R.K., Raskar, S., 2021. Non-conservative removal of dissolved rhenium from a coastal lagoon: Clay adsorption versus biological uptake. Chemical Geology 580, 120378. https://doi.org/10.1016/j.chemgeo.2021.120378.
Dellinger, M., Hilton, R.G., Baronas, J.J., Torres, M.A., Burt, E.I., Clark, K.E., Galy, V., Ccahuana Quispe, A.J., West, A.J., 2023. High rates of rock organic carbon oxidation sustained as Andean sediment transits the Amazon foreland-floodplain. Proceedings of the National Academy of Sciences 120(39), e2306343120. https://doi.org/10.1073/pnas.2306343120.
Fuller, A.J., Shaw, S., Peacock, C.L., Trivedi, D., Small, J.S., Abrahamsen, L.G., Burke, I.T., 2014. Ionic strength and pH dependent multi-site sorption of Cs onto a micaceous aquifer sediment. Applied Geochemistry 40, 32-42. https://doi.org/10.1016/j.apgeochem.2013.10.017.
Gaillardet, J., Dupré, B., Louvat, P., Allègre, C.J., 1999. Global silicate weathering and CO2 consumption rates deduced from the chemistry of large rivers. Chemical Geology 159(1), 3-30. https://doi.org/10.1016/S0009-2541(99)00031-5.
Galy, A., France-Lanord, C., 1999. Weathering processes in the Ganges–Brahmaputra basin and the riverine alkalinity budget. Chemical Geology 159(1), 31-60. https://doi.org/10.1016/S0009-2541(99)00033-9.
Galy, V., Beyssac, O., France-Lanord, C., Eglinton, T., 2008a. Recycling of Graphite During Himalayan Erosion: A Geological Stabilization of Carbon in the Crust. Science 322(5903), 943-945. https://doi.org/10.1126/science.1161408.
Galy, V., France-Lanord, C., Beyssac, O., Faure, P., Kudrass, H., Palhol, F., 2007. Efficient organic carbon burial in the Bengal fan sustained by the Himalayan erosional system. Nature 450(7168), 407-410. https://doi.org/10.1038/nature06273.
Galy, V., France-Lanord, C., Lartiges, B., 2008b. Loading and fate of particulate organic carbon from the Himalaya to the Ganga–Brahmaputra delta. Geochimica et Cosmochimica Acta 72(7), 1767-1787. https://doi.org/10.1016/j.gca.2008.01.027.
Galy, V., Peucker-Ehrenbrink, B., Eglinton, T., 2015. Global carbon export from the terrestrial biosphere controlled by erosion. Nature 521(7551), 204-207. https://doi.org/10.1038/nature14400.
Ghazi, L., Grant, K.E., Chappaz, A., Danish, M., Peucker-Ehrenbrink, B., Pett-Ridge, J.C., 2024. The Global Biogeochemical Cycle of Rhenium. Global Biogeochemical Cycles 38(10), e2024GB008254. https://doi.org/10.1029/2024GB008254.
Grant, K.E., Dellinger, M., Dickson, A.J., Ogric, M., Horan, K., Petsch, S., Hilton, R.G., 2025. Validating the rhenium proxy for rock organic carbon oxidation using weathering profiles. Chemical Geology 671, 122464. https://doi.org/10.1016/j.chemgeo.2024.122464.

Gu, X., Rempe, D.M., Dietrich, W.E., West, A.J., Lin, T.-C., Jin, L., Brantley, S.L., 2020. Chemical reactions, porosity, and microfracturing in shale during weathering: The effect of erosion rate. Geochimica et Cosmochimica Acta 269, 63-100. https://doi.org/10.1016/j.gca.2019.09.044.

Hemingway, J.D., Hilton, R.G., Hovius, N., Eglinton, T.I., Haghipour, N., Wacker, L., Chen, M.-C., Galy, V.V., 2018. Microbial oxidation of lithospheric organic carbon in rapidly eroding tropical mountain soils. Science 360(6385), 209-212. https://doi.org/10.1126/science.aao6463.

Hilton, R.G., Gaillardet, J., Calmels, D., Birck, J.-L., 2014. Geological respiration of a mountain belt revealed by the trace element rhenium. Earth and Planetary Science Letters 403, 27-36. https://doi.org/10.1016/j.epsl.2014.06.021.

Hilton, R.G., Galy, A., Hovius, N., 2008. Riverine particulate organic carbon from an active mountain belt: Importance of landslides. Global Biogeochemical Cycles 22(1). https://doi.org/10.1029/2006GB002905.

Hilton, R.G., Galy, V., Gaillardet, J., Dellinger, M., Bryant, C., O'Regan, M., Gröcke, D.R., Coxall, H., Bouchez, J., Calmels, D., 2015. Erosion of organic carbon in the Arctic as a geological carbon dioxide sink. Nature 524(7563), 84-87. https://doi.org/10.1038/nature14653.

Hilton, R.G., Turowski, J.M., Winnick, M., Dellinger, M., Schleppi, P., Williams, K.H., Lawrence, C.R., Maher, K., West, M., Hayton, A., 2021. Concentration-Discharge Relationships of Dissolved Rhenium in Alpine Catchments Reveal Its Use as a Tracer of Oxidative Weathering. Water Resources Research 57(11), e2021WR029844. https://doi.org/10.1029/2021WR029844.

Hodge, V.F., Johannesson, K.H., Stetzenbach, K.J., 1996. Rhenium, molybdenum, and uranium in groundwater from the southern Great Basin, USA: Evidence for conservative behavior. Geochimica et Cosmochimica Acta 60(17), 3197-3214. https://doi.org/10.1016/0016-7037(96)00183-4.

Horan, K., Hilton, R.G., Dellinger, M., Tipper, E., Galy, V., Calmels, D., Selby, D., Gaillardet, J., Ottley, C.J., Parsons, D.R., Burton, K.W., 2019. Carbon dioxide emissions by rock organic carbon oxidation and the net geochemical carbon budget of the Mackenzie River Basin. American Journal of Science 319(6), 473-499. https://doi.org/10.2475/06.2019.02.

Horan, K., Hilton, R.G., Selby, D., Ottley, C.J., Grocke, D.R., Hicks, M., Burton, K.W., 2017. Mountain glaciation drives rapid oxidation of rock-bound organic carbon. Sci Adv 3(10), e1701107. https://doi.org/10.1126/sciadv.1701107.

IMD, 2013. Rainfall Statistics of India - 2012. https://hydro.imd.gov.in/hydrometweb/(S(jumig145msssex55bdywog55))/PRODUCTS/Publications/Rainfall%20Statistics%20of%20India%20-%202012/Rainfall%20Statistics%20of%20India%20-%202012.pdf. (accessed 12/02/2026.

IMD, 2014. Rainfall Statistics of India - 2013. https://hydro.imd.gov.in/hydrometweb/(S(jumig145msssex55bdywog55))/PRODUCTS/Publications/Rainfall%20Statistics%20of%20India%20-%202012/Rainfall%20Statistics%20of%20India%20-%202012.pdf. (accessed (12/02/2026).

IMD, 2016a. Rainfall Statistics of India - 2014. https://hydro.imd.gov.in/hydrometweb/(S(jumig145msssex55bdywog55))/PRODUCTS/Publications/Rainfall%20Statistics%20of%20India%20-%202012/Rainfall%20Statistics%20of%20India%20-%202012.pdf. (accessed 12/02/2026.

IMD, 2016b. Rainfall Statistics of India - 2015. https://hydro.imd.gov.in/hydrometweb/(S(jumig145msssex55bdywog55))/PRODUCTS/Publications/Rainfall%20Statistics%20of%20India%20-%202012/Rainfall%20Statistics%20of%20India%20-%202012.pdf. (accessed 12/02/2026.

IMD, 2017. Rainfall Statistics of India - 2016. https://hydro.imd.gov.in/hydrometweb/(S(jumig145msssex55bdywog55))/PRODUCTS/Publications/Rainfall%20Statistics%20of%20India%20-%202012/Rainfall%20Statistics%20of%20India%20-%202012.pdf. (accessed 12/02/2026.
IMD, 2018. Rainfall Statistics of India - 2017. https://hydro.imd.gov.in/hydrometweb/(S(jumig145msssex55bdywog55))/PRODUCTS/Publications/Rainfall%20Statistics%20of%20India%20-%202012/Rainfall%20Statistics%20of%20India%20-%202012.pdf. (accessed 12/02/2026.
IMD, 2020. Rainfall Statistics of India - 2018. https://hydro.imd.gov.in/hydrometweb/(S(jumig145msssex55bdywog55))/PRODUCTS/Publications/Rainfall%20Statistics%20of%20India%20-%202012/Rainfall%20Statistics%20of%20India%20-%202012.pdf. (accessed 12/02/2026.
IMD, 2021a. Rainfall Statistics of India - 2019. https://hydro.imd.gov.in/hydrometweb/(S(jumig145msssex55bdywog55))/PRODUCTS/Publications/Rainfall%20Statistics%20of%20India%20-%202012/Rainfall%20Statistics%20of%20India%20-%202012.pdf. (accessed 12/02/2026.
IMD, 2021b. Rainfall Statistics of India - 2020. https://hydro.imd.gov.in/hydrometweb/(S(jumig145msssex55bdywog55))/PRODUCTS/Publications/Rainfall%20Statistics%20of%20India%20-%202012/Rainfall%20Statistics%20of%20India%20-%202012.pdf. (accessed 12/02/2026.
Jaffe, L.A., Peucker-Ehrenbrink, B., Petsch, S.T., 2002. Mobility of rhenium, platinum group elements and organic carbon during black shale weathering. Earth and Planetary Science Letters 198(3), 339-353. https://doi.org/10.1016/S0012-821X(02)00526-5.
Jana, N.C., Bandyopadhyay, S., Ghosh, P.K., Mukhopadhyay, R., 2021. Changing Rainfall Patterns and Their Linkage to Floods in Bhagirathi-Hooghly Basin, India: Implications for Water Resource Management, in: Pandey, B.W., Anand, S. (Eds.), Water Science and Sustainability. Springer International Publishing, Cham, pp. 169-181. doi.org/https://doi.org/10.1007/978-3-030-57488-8_13.
John, D., Seal Ii, R.R., Polyak, D.E., 2017. Rhenium, in: Schulz, K., DeYoung, Jr., Seal, I.I.R.R., Bradley, D. (Eds.), Professional Paper. Reston, VA, p. 62.
Kabata-Pendias, A., Pendias, H., 2001. Soil constituents, in: Kabata-Pendias, A., Pendias, H. (Eds.), Trace elements in soils and plants. CRC Press, pp. 43-64.
Kaste, J.M., Lauer, N.E., Spaetzel, A.B., Goydan, C., 2016. Cosmogenic 22Na as a steady-state tracer of solute transport and water age in first-order catchments. Earth and Planetary Science Letters 456, 78-86. https://doi.org/10.1016/j.epsl.2016.10.002.
Khan, S., Sinha, R., Whitehead, P., Sarkar, S., Jin, L., Futter, M.N., 2018. Flows and sediment dynamics in the Ganga River under present and future climate scenarios. Hydrological Sciences Journal 63(5), 763-782. https://doi.org/10.1080/02626667.2018.1447113.
Koide, M., Hodge, V.F., Yang, J.S., Stallard, M., Goldberg, E.G., Calhoun, J., Bertine, K.K., 1986. Some comparative marine chemistries of rhenium, gold, silver and molybdenum. Applied Geochemistry 1(6), 705-714. https://doi.org/10.1016/0883-2927(86)90092-2.
Krishnaswami, S., Singh, S.K., 1998. Silicate and carbonate weathering in the drainage basins of the Ganga--Ghaghara--Indus headwaters: contributions to major ion and Sr isotope geochemistry. Proceedings of the Indian Academy of Sciences--Earth and Planetary Sciences 107(4), 283-291.
Kumar, P., Saikia, L., Meenakshi, Khandelwal, D., Kumar, P.V., Sharma, R., Ojha, S., Gargari, S., Mukherjee, P.K., Chopra, S., 2022. Statistical assessment of long-term performance for AMS

measurements at IUAC, New Delhi. Nuclear Instruments and Methods in Physics Research Section B: Beam Interactions with Materials and Atoms 529, 29-37. https://doi.org/10.1016/j.nimb.2022.08.008.
Lien, W.-Y., Chen, C.-T., Lee, Y.-H., Su, C.-C., Wang, P.-L., Lin, L.-H., 2025. Two-stage oxidation of petrogenic organic carbon in a rapidly exhuming small mountainous catchment. Communications Earth & Environment 6(1), 45. https://doi.org/10.1038/s43247-025-02015-8.
Lupker, M., Blard, P.-H., Lavé, J., France-Lanord, C., Leanni, L., Puchol, N., Charreau, J., Bourlès, D., 2012a. 10Be-derived Himalayan denudation rates and sediment budgets in the Ganga basin. Earth and Planetary Science Letters 333-334, 146-156. https://doi.org/10.1016/j.epsl.2012.04.020.
Lupker, M., France-Lanord, C., Galy, V., Lavé, J., Gaillardet, J., Gajurel, A.P., Guilmette, C., Rahman, M., Singh, S.K., Sinha, R., 2012b. Predominant floodplain over mountain weathering of Himalayan sediments (Ganga basin). Geochimica et Cosmochimica Acta 84, 410-432. https://doi.org/10.1016/j.gca.2012.02.001.
Lupker, M., France-Lanord, C., Lartiges, B., 2016. Impact of sediment–seawater cation exchange on Himalayan chemical weathering fluxes. Earth Surf. Dynam. 4(3), 675-684. 10.5194/esurf-4-675-2016.
Lupker, M., France-Lanord, C., Lavé, J., Bouchez, J., Galy, V., Métivier, F., Gaillardet, J., Lartiges, B., Mugnier, J.-L., 2011. A Rouse-based method to integrate the chemical composition of river sediments: Application to the Ganga basin. Journal of Geophysical Research: Earth Surface 116(F4). https://doi.org/10.1029/2010JF001947.
Majumdar, A., Satpathy, J., Kayee, J., Das, R., 2020. Trace metal composition of rainwater and aerosol from Kolkata, a megacity in eastern India. SN Applied Sciences 2(12), 2122. https://doi.org/10.1007/s42452-020-03933-2.
Miller, C.A., Peucker-Ehrenbrink, B., Walker, B.D., Marcantonio, F., 2011. Re-assessing the surface cycling of molybdenum and rhenium. Geochimica et Cosmochimica Acta 75(22), 7146-7179. https://doi.org/10.1016/j.gca.2011.09.005.
Mondal, G.C., Singh, A.K., Singh, T.B., 2018. Damodar River Basin: Storehouse of Indian Coal, in: Singh, D.S. (Ed.) The Indian Rivers: Scientific and Socio-economic Aspects. Springer Singapore, Singapore, pp. 259-272. doi.org/https://doi.org/10.1007/978-981-10-2984-4_21.
Mukhopadhyay, A., Acharyya, R., Habel, M., Pal, I., Pramanick, N., Hati, J.P., Sanyal, M.K., Ghosh, T., 2023. Upstream River Erosion vis-a-vis Sediments Variability in Hugli Estuary, India: A Geospatial Approach. Water 15(7), 1285. https://doi.org/10.3390/w15071285.
Němec, M., Wacker, L., Gäggeler, H., 2010. Optimization of the Graphitization Process at Age-1. Radiocarbon 52(3), 1380-1393. https://doi.org/10.1017/S0033822200046464.
Nesbitt, H.W., Young, G.M., 1982. Early Proterozoic climates and plate motions inferred from major element chemistry of lutites. Nature 299(5885), 715-717. https://doi.org/10.1038/299715a0.
Nikolaychuk, P.A., 2022. The potential—pH diagram for rhenium. Chemical Thermodynamics and Thermal Analysis 7, 100068. https://doi.org/10.1016/j.ctta.2022.100068.
Park, S.-M., Alessi, D.S., Baek, K., 2019. Selective adsorption and irreversible fixation behavior of cesium onto 2:1 layered clay mineral: A mini review. Journal of Hazardous Materials 369, 569-576. https://doi.org/10.1016/j.jhazmat.2019.02.061.
Pearson, D.G., Irvine, G.J., Ionov, D.A., Boyd, F.R., Dreibus, G.E., 2004. Re–Os isotope systematics and platinum group element fractionation during mantle melt extraction: a study of massif and xenolith peridotite suites. Chemical Geology 208(1), 29-59. https://doi.org/10.1016/j.chemgeo.2004.04.005.

Peucker-Ehrenbrink, B., Hannigan, R.E., 2000. Effects of black shale weathering on the mobility of rhenium and platinum group elements. Geology 28(5), 475-478. https://doi.org/10.1130/0091-7613(2000)28<475:EOBSWO>2.0.CO;2.
Peucker-Ehrenbrink, B., Jahn, B.-m., 2001. Rhenium-osmium isotope systematics and platinum group element concentrations: Loess and the upper continental crust. Geochemistry, Geophysics, Geosystems 2(10). https://doi.org/10.1029/2001GC000172.
Pierson-Wickmann, A.-C., Reisberg, L., France-Lanord, C., 2000. The Os isotopic composition of Himalayan river bedloads and bedrocks: importance of black shales. Earth and Planetary Science Letters 176(2), 203-218. https://doi.org/10.1016/S0012-821X(00)00003-0.
Pierson-Wickmann, A.-C., Reisberg, L., France-Lanord, C., 2002. Behavior of Re and Os during low-temperature alteration: Results from Himalayan soils and altered black shales. Geochimica et Cosmochimica Acta 66(9), 1539-1548. https://doi.org/10.1016/S0016-7037(01)00865-1.
Rahaman, W., Singh, S.K., 2010. Rhenium in rivers and estuaries of India: Sources, transport and behaviour. Marine Chemistry 118(1), 1-10. https://doi.org/10.1016/j.marchem.2009.09.008.
Rahaman, W., Singh, S.K., Shukla, A.D., 2012. Rhenium in Indian rivers: Sources, fluxes, and contribution to oceanic budget. Geochemistry, Geophysics, Geosystems 13(8). https://doi.org/10.1029/2012GC004083.
Rajan, K., Khudsar, F.A., Kumar, R., 2023. Spatio-temporal patterns of microplastic contamination in surface waters of Hooghly River Estuary: Causes and consequences. Regional Studies in Marine Science 65, 103111. https://doi.org/10.1016/j.rsma.2023.103111.
Rout, R.K., Tripathy, G.R., 2024. Net effect of chemical erosion in a tropical basin on carbon cycle: Constraints from elemental and sulfur isotopic composition of the Mahanadi river water. Chemical Geology 644, 121859. https://doi.org/10.1016/j.chemgeo.2023.121859.
Roy, N.G., Sinha, R., 2017. Linking hydrology and sediment dynamics of large alluvial rivers to landscape diversity in the Ganga dispersal system, India. Earth Surface Processes and Landforms 42(7), 1078-1091. https://doi.org/10.1002/esp.4074.
Rudra, K., 2014. Changing river courses in the western part of the Ganga–Brahmaputra delta. Geomorphology 227, 87-100. https://doi.org/10.1016/j.geomorph.2014.05.013.
Sadhuram, Y., Sarma, V.V., Murthy, T.V.R., Rao, B.P., 2005. Seasonal variability of physico-chemical characteristics of the Haldia channel of Hooghly estuary, India. Journal of Earth System Science 114(1), 37-49. https://doi.org/10.1007/BF02702007.
Samanta, S., Dalai, T.K., 2016. Dissolved and particulate Barium in the Ganga (Hooghly) River estuary, India: Solute-particle interactions and the enhanced dissolved flux to the oceans. Geochimica et Cosmochimica Acta 195, 1-28. https://doi.org/10.1016/j.gca.2016.09.005.
Samanta, S., Dalai, T.K., 2018. Massive production of heavy metals in the Ganga (Hooghly) River estuary, India: Global importance of solute-particle interaction and enhanced metal fluxes to the oceans. Geochimica et Cosmochimica Acta 228, 243-258. https://doi.org/10.1016/j.gca.2018.03.002.
Samanta, S., Dalai, T.K., Pattanaik, J.K., Rai, S.K., Mazumdar, A., 2015. Dissolved inorganic carbon (DIC) and its δ13C in the Ganga (Hooghly) River estuary, India: Evidence of DIC generation via organic carbon degradation and carbonate dissolution. Geochimica et Cosmochimica Acta 165, 226-248. https://doi.org/10.1016/j.gca.2015.05.040.
Sarkar, S.K., Frančišković-Bilinski, S., Bhattacharya, A., Saha, M., Bilinski, H., 2004. Levels of elements in the surficial estuarine sediments of the Hugli River, northeast India and their environmental implications. Environment International 30(8), 1089-1098. https://doi.org/10.1016/j.envint.2004.06.005.

Scheingross, J.S., Hovius, N., Dellinger, M., Hilton, R.G., Repasch, M., Sachse, D., Gröcke, D.R., Vieth-Hillebrand, A., Turowski, J.M., 2019. Preservation of organic carbon during active fluvial transport and particle abrasion. Geology 47(10), 958-962. https://doi.org/10.1130/G46442.1.
Schlitzer, R., 2021. Ocean Data View (Version 5.5.2). doi.org/https://odv.awi.de.
Sharma, R., Umapathy, G.R., Kumar, P., Ojha, S., Gargari, S., Joshi, R., Chopra, S., Kanjilal, D., 2019. AMS and upcoming geochronology facility at Inter University Accelerator Centre (IUAC), New Delhi, India. Nuclear Instruments and Methods in Physics Research Section B: Beam Interactions with Materials and Atoms 438, 124-130. https://doi.org/10.1016/j.nimb.2018.07.002.
Sinclair, W.D., Jonasson, I.R., Kirkham, R.V., Soregaroli, A.E., 2016. Rhenium in Canadian mineral deposits. Geological Survey of Canada, Ottawa, Canada.
Singh, S.K., Rai, S.K., Krishnaswami, S., 2008. Sr and Nd isotopes in river sediments from the Ganga Basin: Sediment provenance and spatial variability in physical erosion. Journal of Geophysical Research: Earth Surface 113(F3). https://doi.org/10.1029/2007JF000909.
Singh, S.K., Trivedi, J.R., Krishnaswami, S., 1999. Re-Os isotope systematics in black shales from the Lesser Himalaya: their chronology and role in the 187Os/188Os evolution of seawater. Geochimica et Cosmochimica Acta 63(16), 2381-2392. https://doi.org/10.1016/S0016-7037(99)00201-X.
Sinha, R., Jain, V., Babu, G.P., Ghosh, S., 2005. Geomorphic characterization and diversity of the fluvial systems of the Gangetic Plains. Geomorphology 70(3), 207-225. https://doi.org/10.1016/j.geomorph.2005.02.006.
Stolze, L., Dwivedi, D., Steefel, C., Molins, S., Dong, W., Beutler, C., Newman, A., Williams, K., 2026. Model-Based Interpretation of Solute Exports and Carbon Partitioning During Shale Weathering in a Mountainous Hillslope. 62(3), e2025WR041597. https://doi.org/10.1029/2025WR041597.
Stüeken, E.E., de Castro, M., Krotz, L., Brodie, C., Iammarino, M., Giazzi, G., 2020. Optimized switch-over between CHNS abundance and CNS isotope ratio analyses by elemental analyzer-isotope ratio mass spectrometry: Application to six geological reference materials. Rapid Communications in Mass Spectrometry 34(18), e8821. https://doi.org/10.1002/rcm.8821.
Tanaka, K., Kozai, N., Ohnuki, T., Grambow, B., 2019. Study on coordination structure of Re adsorbed on Mg–Al layered double hydroxide using X-ray absorption fine structure. Journal of Porous Materials 26(2), 505-511. https://doi.org/10.1007/s10934-018-0634-z.
Taylor, S.R., McLennan, S.M., 1985. The continental crust: Its composition and evolution. Blackwell Scientific Publications, Malden, MA.
Tipper, E.T., Stevenson, E.I., Alcock, V., Knight, A.C.G., Baronas, J.J., Hilton, R.G., Bickle, M.J., Larkin, C.S., Feng, L., Relph, K.E., Hughes, G., 2021. Global silicate weathering flux overestimated because of sediment–water cation exchange. Proceedings of the National Academy of Sciences 118(1), e2016430118. https://doi.org/10.1073/pnas.2016430118.
Tripathy, G.R., Singh, S.K., 2010. Chemical erosion rates of river basins of the Ganga system in the Himalaya: Reanalysis based on inversion of dissolved major ions, Sr, and 87Sr/86Sr. Geochemistry, Geophysics, Geosystems 11(3). https://doi.org/10.1029/2009GC002862.
Varikoden, H., Revadekar, J.V., 2020. On the extreme rainfall events during the southwest monsoon season in northeast regions of the Indian subcontinent. Meteorological Applications 27(1), e1822. https://doi.org/10.1002/met.1822.
Wang, Y., Chen, Y., Li, S., Hedding, D.W., Chen, J., 2025. Carbon Emissions Through the Weathering of Petrogenic Organic Carbon and the Net Geological Carbon Budget of the Tibetan

Plateau. Geophysical Research Letters 52(4), e2024GL110718. https://doi.org/10.1029/2024GL110718.
Wang, Y., Li, S., Xu, P., Wang, H., Chen, Y., Chen, J., 2024. Rapid and significant perturbations on the global geochemical cycle of rhenium by human activities ----- A case study in Yangtze River basin. Applied Geochemistry 162, 105912. https://doi.org/10.1016/j.apgeochem.2024.105912.
Zhang, Y., Wang, J., Qu, Y., Zhu, C., Jin, Z., 2024. Mobility of rhenium and selenium during chemical weathering and their implication for petrogenic organic carbon oxidation. Science China Earth Sciences 67(3), 740-750. https://doi.org/10.1007/s11430-023-1244-5.
Zondervan, J.R., Hilton, R.G., Dellinger, M., Clubb, F.J., Roylands, T., Ogrič, M., 2023. Rock organic carbon oxidation CO2 release offsets silicate weathering sink. Nature 623(7986), 329-333. https://doi.org/10.1038/s41586-023-06581-9.